REPORT DOCUMENTATION PAGE

Form Approved OMB No. 0704-0188

1. REPORT DATE *(DD-MM-YYYY)*	2. REPORT TYPE	3. DATES COVERED *(From – To)*
30-08-2000	Final Report	26 Aug 99 – 01 Jun 01

4. TITLE AND SUBTITLE

Ceramic/Metal Laminate For Application Involving High and Rapid Thermal Gradients

5a. CONTRACT NUMBER
F61775-99-WE067

5b. GRANT NUMBER

5c. PROGRAM ELEMENT NUMBER

6. AUTHOR(S)

Professor Dov Sherman

5d. PROJECT NUMBER

5d. TASK NUMBER

5e. WORK UNIT NUMBER

7. PERFORMING ORGANIZATION NAME(S) AND ADDRESS(ES)

Technion - Israel Institute of Science and Technology
Haifa 32 000
Israel

8. PERFORMING ORGANIZATION REPORT NUMBER

N/A

9. SPONSORING/MONITORING AGENCY NAME(S) AND ADDRESS(ES)

EOARD
PSC 802 BOX 14
FPO 09499-0014

10. SPONSOR/MONITOR'S ACRONYM(S)

11. SPONSOR/MONITOR'S REPORT NUMBER(S)
SPC 99-4067

12. DISTRIBUTION/AVAILABILITY STATEMENT

Approved for public release; distribution is unlimited.

13. SUPPLEMENTARY NOTES

14. ABSTRACT

This report results from a contract tasking Technion - Israel Institute of Science and Technology as follows: The contractor will investigate a novel laminated material system consisting of thin ceramic layers alternating with thinner metallic interlayers for use as flaps in a gas exhaust afterburner. In this system, the ceramic is the high melting point constituent, possessing high stiffness, high wear and fatigue resistance at elevated temperatures. The metal interlayers provide the needed compliance, ductility, and toughness. The interface should be strong enough to prevent crack deflection and disintegration of the material system when damage occurs. Oxidation resistance of such systems is expected to be good due to the small exposed area of the metallic interlayers. Good fracture toughness of the laminated system (more than an order of magnitude better than monolithic alumina) and R-curve behavior upon mechanical loading is expected.

15. SUBJECT TERMS
EOARD, Materials, Thermal Protection & Control, Aeroengines, Ceramics

16. SECURITY CLASSIFICATION OF:			17. LIMITATION OF ABSTRACT	18, NUMBER OF PAGES	19a. NAME OF RESPONSIBLE PERSON
a. REPORT	b. ABSTRACT	c. THIS PAGE			Charles H. Ward, Maj, USAF
UNCLAS	UNCLAS	UNCLAS	UL	57	19b. TELEPHONE NUMBER *(Include area code)* +44 (0)20 7514 3154

Alumina/Nickel Laminate Under Thermal Shock Up to 1000°C.

Dov Sherman
Dept. of Materials Engineering
Technion-Israel Institute of Technology
Haifa, 32000 Israel

ABSTRACT[1]

The mechanical behavior of an alumina/nickel laminate under thermal shock loading was investigated. The maximum thermal shock temperature was 1000°C. The laminate architecture is the cause of a basic change in the cracking mechanisms, manifested in a dramatic increase in the mechanical residual strength over that of monolithic alumina.

The laminated system was constructed by alternating alumina layers with nickel interlayers, and joining them with a combination of liquid state (brazing) and solid state (diffusion) bonding. The material system was tested by water quenching square shaped laminated specimens, from initial at temperatures of up to 1000°C. Three point bending tests revealed the mechanical strength before and after thermal shock, and SEM analysis described the damage mechanisms and the extent of debonding at the nickel/alumina interfaces. A 1-D numerical procedure was developed for analyzing the stress field across the specimen during thermal shock. It revealed the superiority of this material system over monolithic ceramics under thermal shock conditions.

1. INTRODUCTION

When materials are subjected to high thermal gradients or rapid changes in temperatures, high thermal stresses are generated, that may cause large irreversible deformations in ductile materials or cracks in brittle materials such as ceramics. The severe condition is that of thermal shock, especially when the heat transfer coefficient is large, the best example being quenching in water.

A ceramic/metal laminate, a material system for applications involving thermal shock, was investigated and reported lately by the author [1]. In that preliminary study, the ceramic/metal laminate was constructed from 370 μm thick Coor's ADS96R alumina plates alternating with 30-100 μm thick Wesgo Cusil ABA (active braze alloy) interlayer foils, and joined by active brazing. Square shaped laminated plates were quenched in distilled water at room temperature, in which the heat transfer is large. Only the bottom surface off the laminated plates, initially at 600°C and 800°C, were quenched in a specially designed apparatus. The basic features of the architecture were identified: the absence of interaction between the biaxial cracking mechanisms

[1] This material is based upon work supported by the European Office of Aerospace Research and Development, Air Force Office of Scientific Research, Air Force Research Laboratory, under Contract No. F61775-99-WE067.

in a ceramic layer and those in the adjacent ceramic layers, and localization of the damage in those layers that experienced sufficient tensile stresses. The result was a dramatic increase in the residual strength of the laminated system after thermal shock, being more than an order of magnitude higher than that of monolithic alumina under the same conditions of thermal shock and mechanical loading. In addition, R-curve behavior upon mechanical loading due to plastic deformation of the metallic interlayer was observed. Furthermore, the crack density in individual layers decreased as the distance from the quenched surface increases. Another important feature of laminated systems is their ability to combine more than two materials, which reduces the thermal stresses and improves the survivability of the material system under severe thermal shock conditions.

Ceramic/metal laminates were extensively studied in the last two decades, both for their load carrying capacity [2-5] and for their increased fracture toughness [6-10]. Fiber reinforced ceramic matrix composites were investigated for their thermal shock resistance [11, 12], when saturation of the damage after a few thermal cycles was observed. SiC/Graphite [13, 14] laminate was tested [15], and progressive weight loss was observed during thermal shock cycles, resulting in crack deflection and progressive flaking of SiC layers. Ceramic matrix composites were evaluated for their ability to withstand large spatial thermal gradients, and cracking due to high thermal stresses was observed [16,17].

In the current investigation, a ceramic/metal laminate was constructed by alternating alumina plates and nickel foils. This paper deals with the processing, the thermal shock testing, the mechanical evaluations, and SEM analysis, of the laminate constructed from 9 alumina and 8 nickel layers. A numerical analysis is compared with the experimental results, and new temperature/residual stresses map was constructed.

1. EXPERIMENTAL

1.1 Materials

The ceramic layers in this investigation were 2"x2" ADS96R Coor's 96% pure alumina, of a nominal thickness of 380 μm. The metallic interlayers were 25 or 50 μm thick, 99% pure annealed nickel foils, supplied by the Johnson Matthey Co. Nickel was chosen for its relatively high melting point (1453^{O}C), high elastic modulus and high strength, the positive mismatch between its thermal expansion coefficients and that of alumina, and, finally, the relatively simple joining method with alumina. The low cost and availability of the 99% pure nickel foils is an additional advantage.

2.2 Processing

The combined liquid state and solid state joining method (viz. brazing and diffusion bonding) was chosen [18-22], and the following processing route was adopted: The alumina layers were coated on both sides with a 100Å Ti thin film, and then with 2-3 μm of pure copper films by electron beam depositing device. No special surface treatment of the alumina layer was carried out, aside from cleaning them with acetone. The laminated system contain 9 alumina layers (380 μm thick each) and 8 NiCu (nickel/copper) interlayers (each 30 or 55 μm thick NiCu).

Several alumina/NiCu laminates, 2x2 in^2 gage area, were put one on top of the other in a Thermal Technology® Bonding Furnace. The applied time-temperature-pressure-environment relationships are shown in **Fig. 1**. At the first stage, special attention was paid to cleaning the surfaces of the layers involved. Three flushing cycles were carried out, in each of which a 10^{-3} Tor vacuum was achieved. This was followed by a flow of forming gas (Ar+5% H_2). The specimens were kept in the forming gas environment for an hour at $600^{O}C$, free of pressure, and with a low gas flow to the atmosphere. At the end of this stage, the forming gas was switched to Ar only, and pressure was applied. The maximum joining temperature was $1150^{O}C$, which was held for 6 hours, and under maximum applied pressure of 10 MPa, kept up until the laminates had cooled down completely (**Fig. 1**). The thermal and mechanical properties of nickel and alumina are given in **Table 1.** Since copper is fully soluble in nickel, the mechanical and thermal properties of the composition NiCu in the relevant percentages are also shown in **Table 1**, in addition to related properties found in the technical literature.

2.3 Thermal shock loading

The laminates, cut to 23x23 mm^2 plates, were attached to a special stage designed to maintain the specimens horizontally during quenching. A piston drives the stage to a container of distilled water at room temperature, in such a manner that only the bottom surface of the specimen experiences the thermal shock (**Fig. 2a**). Two k-type, 0.15 mm diameter thermocouples, one attached to the to surface of the specimen the other to its bottom surface, measured the in-situ temperature during quenching (**Fig. 2a**). The tip of each thermocouple was ground to a hemispherical shape and attached to the specimen using Cerambond® cement. In order to minimize any influence on the temperature measurements, the total volume of the cement and the tip did not exceed 2 mm^3. The thermocouples were connected to a Thermal Technology© high data acquisition card, having a measuring rate of up to 10KHz.

Bending beams of 3.5 mm nominal width were cut from virgin plates and from plates that had experienced thermal shock loading, for evaluating their mechanical residual strength.

2.4 Evaluating the mechanical strength

Three point bending (3PB) tests of the two types of laminates were carried out before and after thermal shock loading. The specimens were cut from the processed plates or from the plate that had undergone thermal shock. They were all of 3.3 mm nominal width. The total thickness of the laminates averaged 3.9 mm and 3.7 mm for the 55 μm and the 30 μm thick NiCu interlayers, respectively. The specimens were put in a specially designed, fully articulated bending bridge, which enables loading of pure 3PB deformation. The point load velocity was 0.05 mm/min.

2. RESULTS AND DICUSSIONS

2.1 Behavior before thermal shock

SEM analysis of the interface between the alumina and the NiCu after processing demonstrates that full bonding exists and that the interface replicates the morphology of the unpolished alumina layers, **Fig. 3**. The surface roughness is about 5 μm, which is the average grain size, but the thickness of the deposited copper layer was only 2 –3 μm, indicating that plastic deformation of the nickel layers in order to match the alumina morphology occurred during processing.

Load vs. load point deflection curves of typical specimens of the two types of laminates before thermal shock loading are shown in **Fig. 4a and b**. All the specimens of either type exhibited linear load deflection relationships prior to the cracking of the alumina layers [**23**], which suggests that no plastic deformation took place up to these points. All the laminates containing thin NiCu interlayers underwent brittle fracture (**Fig. 4b**), while those with thicker NiCu (**Fig. 4a**) interlayers exhibited energy dissipating mechanisms due to plastic deformation of the metallic interlayers after fracture of the alumina layers. The effective stresses at fracture, $\sigma_{eff} = 3P(2l)/2b(2h)^2$ calculated assuming monolithic and homogenized specimen (where *P, l, h, and b* are, respectively, the load to fracture of the laminate, the span, the total thickness of the specimen, and the width) are also shown in **Figs. 4a and b**.

The gradual plastic deformation of the 55 μm thick NiCu metallic interlayers after mechanical loading of the unquenched laminate is presented in **Figs. 5a to d**. This deformation is the result of crack deflection due to mechanical loading in this configuration. The crack deflection in the laminates with thick metallic interlayers was of the order of the metal layer thickness, and up to 70 μm deflection was observed at the interface between the layers that had developed full plastic deformation. It is evident that the delaminations are dominated by Mode I deformation mechanisms. Views of the plastically deformed metallic interlayers are shown in **Figs. 6a to d**. While the plastic deformation mechanisms in the thin metallic interlayers (Figs. 6a and a magnified view in Fig. 6b) are of the same nature as those in the thicker metallic interlayers (Fig. 6c and a magnified view in Fig. 6d), the total plastic deformation is negligible in the thinner interlayers and very significant in the thicker ones, due to the larger volume of the thicker metallic interlayers involved in the deformation. Note the morphology of the metallic interlayers' surfaces, which is identical to that of the alumina layers.

3.2 The behavior after thermal shock

Time Temperature relationships at the top and the bottom surfaces of a specimen quenched from 1000^{O}C are shown in **Fig. 7a**, the temperature differences, ΔT, between the two surfaces are also shown in **Fig. 7a**. It is noted that the thermocouple measuring the temperature at the bottom surface of the specimen is influenced by the water, and the actual temperature at the bottom surface may therefore be assumed to decrease more moderately. In another test, the lower thermocouple was attached to one side of the specimen, about 0.5 mm from the bottom surface (isolated from water by 10 mm thick alumina 'walls', see below). At this point the temperature drop is indeed more moderate (**Fig. 7b**), but higher gradients are expected at points closer to the bottom surface. It is noted that the minimal temperature difference for initiating cracks in alumina under the same conditions of geometry and loading is less than 100^{O}C [24].

The quenched specimens were cut to bending beams, either for SEM analysis or for mechanical testing. Micrographs of the cross section of a specimen thermally shocked from 1000^{O}C (with no mechanical loading) are shown in **Figs. 8.** A general view is shown in **Fig. 8a**, while **Figs. 8b to d** are larger magnifications of the alumina/NiCu interface. The crack in the metallic interlayers. The driving force for cracking is the high strain energy in the ceramic layers. As a crack propagates in the ceramic layer, the local strain energy vanishes, and so does the driving force for further cracking or plastic deformation in the metallic interlayers. It is also noted that a crack does not propagates to the adjacent layer, which supports the assumption that there is no interaction between cracking mechanisms in adjacent layers.

Load vs. load point deflection relationships of beam specimens, cut from plates that had been subjected to thermal shock loading and then loaded under 3PB are also shown in **Fig. 4a and b**. The specimens with 55 μm thick metallic interlayers underwent thermal shock from 800 and 1000^{O}C (**Fig. 4a**), while those with 30 μm NiCu were subjected to a greater variety of thermal shock temperatures.

No significant differences in the load-deflection curves between the 800^{O}C and the 1000^{O}C thermally shocked specimens (**Fig. 4a**) is evident, but it is a significant observation that no steep load drop occurred (as happened in the unquenched specimen), indicating that presumably most of the alumina layers were fractured under these thermal shock temperatures. An opportunity to estimate the drop in residual strength as a function of varying thermal shock temperatures is shown in **Fig. 4b** for the laminate with thinner metallic interlayers. The effective strength of the damaged laminate is also shown in these figures. This subject is discussed in detail below.

SEM micrographs of the quenched laminates with the thicker metallic interlayers after mechanical loading, as shown in **Figs. 9a to f**, indicate practically the same damage mechanisms, but with a longer crack deflection, estimated at an average of 150 μm, which is responsible for the increased strain energy to fracture due to the increased plastic deformation of the metallic interlayers in the quenched laminates (see load deflection curves in **Figs. 4**). The effect of the thickness of the metallic layers is also well demonstrated in **Figs. 4**. While the overall strain energy absorbed by the thermally shocked laminates with thick metallic interlayers (Fig. 4a) is comparable to that of the unquenched laminate, it is much smaller in laminates with thin metallic interlayers (Fig. 4b).

3.3 Oxidation resistance of the laminate

In addition to withstanding thermal shock loading and yet maintaining reasonable mechanical strength, ceramic/metal laminated systems should also be able to resist oxidation. We studied the oxidation resistance of the alumina/NiCu laminate, before and after thermal shock, by placing beam specimens in an open tube furnace at a temperature of 1000^{O}C. The specimens were weighed with a Sartorius analytical balance having an accuracy of ±1mg, at room temperature, at certain time intervals. The laminate weight gain normalized by the exposed metallic area is shown in **Fig. 10**. The unquenched laminates with 55 μm and with 30 μm thick NiCu interlayers show the same oxidation resistance after 100 hours, with reducing oxidation rate for increasing oxidation time. It may be assumed that oxidation reaches saturation. Oxidation of the laminate with 55 mm thick metallic interlayers shows similar behaviortively, whether quenched from 800^{O}C or from 1000^{O}C, with 0.25 mg/mm^2 and 0.22 mg/mm^2 normalized weight gain,

respectively, as shown in **Fig. 10**. In this case, saturation of oxidation has not yet been achieved, although the rate of oxidation had decreased. The difference between the two behaviors lie in the greater area exposed to oxidation in the laminates that were subjected to thermal shock. The estimated average depth of the oxide layer is also shown in **Fig. 10**. This estimation was obtained by assuming the density of the oxide film is 6.14 gr/cm^3 (the density of NiO). Note that after 100 hr of oxidation in air at 1000^{O}C, before thermal shock cracking, the depth of the oxide layers is was of the order of 15 μm. The average depth of the thermally shocked specimen is greater, due to the greater free surfaces of the new cracks, which were not considered in the calculations.

SEM micrographs of the oxide layers are shown in **Figs. 11**. The typical cubic crystal structure of the NiO, shown in **Fig. 11a**, contains a brittle crack traversing the layer. Higher magnification of the oxide layer reveals periodic transverse cracks, with crack spacing comparable to the layer thickness, as shown in **Fig. 11b**. This indicates a fully brittle behavior of the oxide layer, which has a strong interface with the metallic NiCu. The oxide layer can be continuous (**Fig. 11c**) or cracked (**Fig. 11d**), presumably resulting from the increased local deformation of the oxide layer in the vicinity of cracked alumina layers.

3.4 Cracking of the alumina layers and edge effect in thermal shock experiments

Optical scans of a specimen that was quenched from 1000^{O}C are shown in **Figs. 12a and b**, the first depicting the quenched surface, with 2-D cracking mechanisms. The crack spacing is comparable to the alumina layers' thickness. The cracks are equally distributed over this surface. A previous investigation of other ceramic/metal laminates [1] under thermal shock loading showed decreasing crack density the greater the distance of the alumina layer from the quenched surface. **Fig. 12b** is an optical scan of the top surface. Although it was expected that no cracks could be generated in this surface, an edge effect was engendered during quenching. The result are long cracks, initiated at the edges of the specimen and propagating toward the center. Six of these cracks crossed all the alumina layers in the specimen, as shown in **Fig. 12b**. It is suggested that the driving force for the initiation and propagation of these cracks is a combination of the rapid heat transfer through the bottom surface (in the z direction), and an in-plane heat transfer from the edges of the specimens. Therefore, a super-position of the thermal stresses from both driving forces is obtained, causing increased damage. To overcome the heat transfer from the edges, specimens were protected by gluing 1 mm and 10 mm thick alumina 'walls' to the edges of the specimen, using Cerambond© glue, which, however, exerted only a moderate influence on the failure loads. Furthermore, an attempt to generate thermal shock conditions by cooling the bottom surface with running water yielded practically the same results. This behavior is a cause of error in the numerical calculations described in the following chapter.

SEM analysis of the quenched alumina layer that has been in contact with the water revealed the cracking mechanisms of that layer: while a minor crack has only very limited opening, the opening of a major crack (generated presumably by to the side effect, **Fig. 12b**) is wide, as shown in **Fig. 12c**. The thermal shock cracks are mixed intergranular and intragranular, progressively generated as the temperature differences increase during thermal shock. Fresh cracks occur nearly perpendicular to one already existing (**Fig. 12d**), this being the most efficient way to reduce the strain energy in the strained material. As is shown in **Fig. 12c and d**, a

bridging phenomenon was observed in the thermally shocked alumina, in which a single grain is bridging the crack surfaces, causing a pull-out effect. An enlargement of a single grain bridging the crack is shown in **Fig. 12f**. This phenomenon may be responsible for R-curve behavior of the alumina layers (within the laminate) under thermal shock, which is usually completely brittle.

4. NUMERICAL ANALYSIS

4.1 Modeling of the thermal problem

The present boundary value problem is that of an infinite square shaped laminated plate, lying in the x,y plane and thermally shocked only at the bottom surface, z=b. We assume that as a result of the thermal shock loading, in-plane biaxial tensile-compressive loads and biaxial bending moments are generated. The analysis of a laminated structure under thermal shock is based on the static analysis of a bi material thermostat [25], in which each layer is subjected to a set of biaxial tensile or compressive loads and bending moments [26]. A more general solution for static multimaterial multilayered systems has lately been presented by Bagchi et al [27].

Such a material system consists of n layers, each of an individual thickness, h_n, and there are n-1 interfaces. The number of materials is unlimited, each being defined by its individual mechanical and thermal properties. An individual layer may be constructed with several degrees of freedom. The bonding between two adjacent layers is considered to be strong, and continuity is not violated. The possible formation of product layers is ignored.

The temporal temperature profile across the laminated plate was calculated using the finite differences scheme. The temperature of node i at time t_{p+1} is [28]:

$$T_i(t_{p+1}) = T_i(t_p) + \frac{\Delta\tau}{C_i}\left[\dot{q}_i + \sum_{j=1}^{n}\frac{T_j(t_p) - T_i(t_p)}{R_{ij}}\right] \qquad (1)$$

where $t_{p+1} = (p+1)\Delta\tau$, and $\Delta\tau \le \min\frac{C_i}{\sum_{j=1}^{n+1} R_{ij}^{-1}}$,

is the minimum time interval for the appropriate temperature calculations within a time step. C_i is the heat capacity of a layer ($C_i = c\rho\Delta V$), R_{ij} is the heat transfer resistance across a layer R=1/hA. $\dot{q}$ is the heat flux generated in a layer, which in thermal shock problems is null. It is noted that the thermal resistance of the interface between two materials was also considered as null. The temperature profiles were calculated regardless of the stresses.

The temporal stresses in an individual layer are the result of in-plane, equal, and uniformly distributed temporal forces, P, which act along the neutral axis of the layer, parallel to the x and y axes, and of temporal equal moments, M, uniformly distributed along the edges of the plate [26]. The equilibrium of temporal forces and moments across the specimen layers dictates:

$$\sum_{i=1}^{n} P_i(t) = 0 \qquad (2)$$

and $$\sum_{i=1}^{n} M_i(t) - \sum_{i=1}^{n-1} P_i(t)\left[\frac{h_i + h_n}{2} + \sum_{k=i+1}^{n-1} h_k\right] = 0 \qquad (3)$$

respectively. The analysis assumes a temporal constant radius of curvature of all the layers [16]:

$$M_i(t) = \kappa(t) D_i(T)(1 + \nu_i(T)) \qquad (4)$$

where $D_i(T) = E_i(T)h_i^3 / 12(1-\nu_i(T)^2)$ is the bending rigidity of a plate, and is a function of temperature. It is noted that $D_i(T)(1+\nu_i) = E_i^{'}(T)I_i$, where $E_i^{'} I_i$ is the bending rigidity of a beam. The kinematic assumption in this calculation arises from strain compatibility across each of the n-1 interfaces, from which follows [25]:

$$\alpha_i(T)\Delta T_i(t) + \frac{P_i(t)}{E_i^{'}(T)h_i} + \frac{h_i\kappa(t)}{2} = \alpha_{i+1}(T)\Delta T_{i+1}(t) + \frac{P_{i+1}(t)}{E_{i+1}^{'}(T)h_{i+1}} - \frac{h_{i+1}\kappa(t)}{2}, \qquad (5)$$

where $\Delta T_i(t)=\Delta T_i(0)-\Delta T_i(t)$ is the temporal temperature difference at a point. The first term on either side of Eq. 5 is the thermal contribution to the total strain in a layer, the second is the tensile contribution, and the third is the contribution of the internal bending moment.

The problem consists of 2n+1 temporal unknowns (n forces, n moments and the radius of curvature) and 2n+1 temporal equations, Eqs. (2) to (5) [18]. The overall solution aims at calculating the internal force vector, Pi. More detailed formulations can be found in [29]. For a known internal force vector, $P_i(t)$, and radius of curvature $\kappa(t)$, the stresses are:

$$\sigma_i(t) = \frac{P_i(t)}{h_i} + \frac{h_i E_i(T)}{2}\kappa(t) \qquad (6)$$

In this investigation, the constituent's mechanical and physical properties used were those at room temperature and assumed to remain constant during the analysis. That assumption is appropriate for ceramics at the analyzed temperatures. Although a reduction in the elastic modulus and thermal properties of the metallic interlayers at increased temperatures is expected, we neglected it for ease of analysis.

It was concluded in Ref.15 that there is no interaction between the cracking mechanisms in an individual layer and that cracking occurs as long as the tensile stresses in that layer exceed the tensile strength of the material. Furthermore, debonding at the metal/ceramic interface is limited and no flaking of layers is expected, hence the temperature distribution does not significantly change after cracking.

When the tensile stresses in an individual brittle layer exceed its tensile strength, σ_{CR}, i.e., when [30-31]

$$\sigma_{xx\ i}(t) = \sigma_{CR} \qquad (7)$$

we assumed that a crack is initiated in the brittle layer, which is thereafter considered as containing a network of biaxial cracks [1] and thus becomes ineffective in sustaining axial forces and bending moments. Therefore the force and the moment of that layer become:

$$P_i(t) = 0 \tag{8a}$$

$$M_i(t) = 0 \tag{8b}$$

and the strain compatibility at the r'th interface obeys:

$$\alpha_i(T)\Delta T_i(t) = \alpha_{i+1}(T)\Delta T_{i+1}(t) + \frac{P_{i+1}(t)}{E'_{i+1}(T)h_{i+1}} - \frac{h_{i+1}\kappa(t)}{2} \tag{9}$$

When a ductile layer is enclosed between two cracked brittle layers, it also becomes ineffective in carrying forces and moments, and Eqs. (8a), (8b) and (9) hold. A MATLAB computer program was built for the analysis.

The residual strength at room temperature of a laminated beam after thermal shock, loaded by three point bending was further analyzed in order to obtain the number of unbroken layers. The procedure is similar to the preceding formulations and is also described in [29]. The material parameters used in the numerical analysis were those presented in **Table 1**.

4.2 Analysis of the zero misfit stresses temperature

The statistical behavior of ceramic/metal laminates was studied in a companion paper [23]. An important outcome of that investigation was the ability to estimate the zero misfit stresses temperature resulting from the thermal processing of the laminates. Using the formulations presented in that investigation, it was found that the thermal residual stresses in the laminates are lower than the maximum stresses predicted by the elastic assumption, where the maximum processing temperature was taken as the zero misfit stresses temperature. This result suggests that stress relaxation due to creep took place upon cooling down, and therefore the zero misfit stresses temperature is lower than the maximum processing temperature. The zero misfit temperatures are 665 and 948^{O}C, for the 55 and the 30 μm thick NiCu interlayers, respectively. It appears that relaxation of the misfit stresses in a constrained thin metallic interlayer is smaller than in a thick one, presumably since stress relaxation due to creep of the metallic interlayers is more difficult in thinner constrained layers. These temperatures are used in the analysis of the laminates under thermal shock, described in the following chapter.

4.3 Results

The program for calculating the stresses in the laminated system under thermal shock considers the thermal residual stresses resulting from a mismatch in the coefficients of thermal expansion. There are three characteristic temperatures: the zero misfit stress temperature (665 and 948 ^{O}C for the laminates containing 55 and 30 μm thick Ni/Cu interlayers, respectively), the room temperature quenching medium (20^{O}C) and the quenching temperature. Each ceramic layer

was modeled by 10 elements, the metallic interlayer by 5. The ceramic layer that experienced the thermal shock was modeled by 35 elements.

Predictions of the behavior of materials under thermal shock must be based on a precise knowledge of their thermal and mechanical properties, and in particular their variation with temperature. Large variations in the heat transfer coefficient between alumina and water with temperature have been reported [32,33]. No data exist for the heat transfer coefficient when alumina at high temperature encounters room temperature water. Based on a previous analysis [24], it was decided that a constant heat transfer coefficient of $6{\cdot}10^4$ W/m^{O}C will use for the analysis.

The stress distributions in both laminates at the end of the fracture process, initiated by thermal shock from 1000^{O}C are shown in **Fig. 13a and b**, for a laminate with 55 and 30 μm thick metallic interlayers, respectively. The strength of an individual alumina layer in both calculations was fixed at 400 MPa. The program terminates when the tensile stress in the first unbroken alumina layer is starting to drop. Three alumina layers were fractured in the laminate with thick metallic interlayers, two in that with thin interlayers, resulting from the low zero misfit stress temperature, which significantly reduces the compressive stresses in the alumina. The effect of the low zero misfit stress temperature is also demonstrated by the large compressive stresses in the metallic interlayers, shown in **Fig. 13a**. The stress distribution profile in the fractured laminate follows that in monolithic ceramics: a tensile-compressive-tensile sequence resulting from the internal moment exists under thermal shock [34].

The number of broken alumina layers due to thermal shock dictates the residual strength of the laminate after the shock. The numerical procedure calculates the externally applied loads to a beam as a function of the strength of the individual alumina layers, which was selected to range between 200 to 400 MPa, values that represent the span of strength of a typical alumina, for varying numbers of broken layers in a laminate. Comparison between the failure loads obtained during bending tests and the numerical analysis enables prediction of the number of broken layers. Since the quenched laminated plates were cut to beams available for bending, the analysis is now that of beams under plane stress conditions. Several assumptions form the basis of the calculations: (i) the damage due to thermal shock loading is that of a network of dense biaxial cracks, (ii) after quenching, the cracked ceramic layers are ineffective in carrying external loads and moments, and the thermal residual stresses are relaxed, (iii) the strength of an individual uncracked ceramic layer is constant (neglecting the statistical nature of strength), (iv) the thermal residual stresses are updated for the changing lay-ups, and (v) linear elasticity is assumed (and extensively discussed in 30N). The formulations are extensively described in [29]. The procedure of the numerical analysis is as follows: The outermost alumina layer iled first. Thereafter, pairs of metal and ceramic layers failed. The applied loads as a function of the strength of the outermost unfailed ceramic layer are shown in **Figs. 14a and b** for the laminates with thick and thin metallic interlayers, respectively. The corresponding normalized loads, or alternatively, the effective strength, σ_{eff} (see section 3.1), under 3PB, are also shown in **Figs. 14a and b**. These are important for engineering purposes. The numbers in Figs. 14a and b indicate the number of broken layers. The bold dashed line corresponds to the load to fracture of the unquenched laminate, while the other bold lines pertain to the reduced laminates in which the outer surface is a metallic layer. The other vertical and horizontal dashed construction lines describe the experimental results. Assuming that the strength of the alumina layers in the

laminate shown in **Fig. 14a** 300 MPa, the load to fracture of the undamaged laminate is 605 N, and the effective strength is 365 MPa while, if one layer is broken, the load to fracture and the effective strength are 544N and 332 MPa, respectively. With the same rationale, if 4 alumina layers are broken, the load carrying capacity of that laminate is 230 N and the effective strength is 140 MPa.

The advantage of the laminated system over monolithic ceramic under thermal shock conditions is well demonstrated in **Fig. 15**, where maps of the room temperature residual strength as a function of thermal shock temperatures and the number of broken alumina layers is shown. Assuming, again, that the strengths of the alumina layers ranged between 200 and 400 MPa, combining the procedures to calculate the number of broken layers during thermal shock (shown in **Figs. 13**), and the residual strength of a laminate with broken alumina layers (**Figs. 14**) had yielded the unforeseen step-like strength temperature relationship, **Fig. 15**. This is the result of the unique damage mechanisms typical of the material system under discussion. The effect of the thermal residual stresses generated during the processing of materials with different thermal expansion coefficients, is also shown in Fig. 15: the unquenched strength is higher than the strength of the individual alumina layers.

The solid and the dashed lines correspond to the laminates containing 55 and 30 μm thick NiCu interlayers, respectively. The numbers refer to the numbers of broken alumina layers, and the dots and dashes line schematically describe the expected behavior of monolithic alumina under thermal shock. The circular and the square symbols pertain to the experimental results of the laminate with thin and thick metallic interlayers, respectively. The discrepancy in the strength temperature relationship between the experimental results and the numerical model is presumably caused by the edge effect existing in small specimens. This effect is likely to vanish for larger laminated plates. The strength of the unquenched laminates, however, is well within the range predicted by the numerical model. Both laminate may be considered to behave practically alike, with an advantage to the laminate containing thin metallic interlayers at temperatures above $850^{O}C$ for the low strength alumina layers and above $1000^{O}C$ for high strength alumina layers.

5. THE BEHAVIOR OF THE LAMINATE UNDER SPATIAL THERMAL GRADIENTS

The aim of the current work, in addition to the exploration of the behavior under thermal shock, was to investigate the behavior of the laminate under severe steady state spatial thermal gradients. This condition is required in the examination of the functioning of the laminate as flaps in jet engine afterburners, which operate in the presence of high spatial thermal gradients. At steady state, these may generate thermal stresses, sufficient to cause catastrophic failure of the flaps. An experimental procedure was accordingly established for this examination.

The laminated specimens were constructed from 6 layers of alumina and 5 NiCu interlayers, fabricated by the processing route described above. The laminate size available for testing was 45X45 mm^2, the total thickness is 2.4 mm and 2.6 mm for laminates containing 30 and 55 NiCu interlayers. The edges of the specimens were cut with a diamond wheel cutter to improve the surface morphology after processing. The specimens were put freely and horizontally on four 2 mm diameter alumina pins, to assure free boundary conditions. Four

thermocouples were glued to the specimens' surfaces, three on the top surface, located at Y=4, 8, and 12 mm, points B,C, and D in **Fig. 16a and b**, one on the bottom surface, at Y=0 (point A in Fig. 16b), in order to capture the temperature field across the specimens.

A super Kantahl heating elements, 2 mm by diameter, was used as the heat source in these experiments. The heating element was located at 0.5 and 3 mm above the top surface of the specimens, along the X axis and at Y=0 (Fig. 16a). The temperature of the heating element was gradually increased by changing the voltage by increments of 10 V each. The voltage was changed only after the temperatures measured by the thermocouples had reached steady state.

Monolithic alumina specimens with the same dimensions as of the laminates were tested as a reference. They were fractured spontaneously by a single crack initiated at one edge of the specimens, propagated along the X direction, underneath and parallel to the heating element. The temperatures measured by the thermocouples at fracture are shown in and **Fig. 17**.

The laminated specimens were fractured at temperatures slightly above those of the monolithic alumina specimens, see **Fig. 17**. Examination of the top and the bottom surfaces of the specimens revealed two stably propagating cracks, emanating from the two edges of the specimens (at Y=0) and advancing stably toward the center of the specimens. The specimens were not cut, and it is therefore yet impossible to decide whether the cracks traverse the inner alumina layers, although cracks appear on the edges of the specimens.

We conclude, although without rigorous analysis, that the thermal gradients in the Y direction, in conjunction with the thermal gradient in the Z direction and especially at Y~0, are very high, so that the generated stresses reached the strength of the ceramic layers at relatively low temperature measured at points A, B, C, and D. The experimental set-up that included a relatively small size laminate, heated by low diameter and high temperature heat source, are the cause of the large thermal gradients near the center of the specimens. Several other heat sources were examined in this investigation, especially different types of halogen lamps, but these caused only very moderate temperature gradients (although with similar temperatures at the measured points), and no damage. We recommend to continue the search for a more appropriate set-up that would match the required conditions of temperature field and stresses in the specimens. Finite element analysis of the laminate under this type of loading is recommended as well.

6. SUMMARY

The mechanical behavior of an alumina/NiCu laminate under thermal shock loading was investigated. The thermal shock loading was achieved by driving laminates in horizontal position, initially at a temperature of up to $1000^{O}C$, into a container of distilled water. The thermal shock was applied only at the bottom surface of the specimens. Several important conclusions are drawn from this investigation:

(i) Very limited crack opening displacement is evident in thermally shocked alumina layers, resulting from the vanishing strain energy as cracks traversing a strained region. In this regard, it is noted that contraction of the metal interlayers at room temperature may cause crack closure.

(ii) Only negligible crack deflections along the NiCu alumina interface are evident after thermal shock loading, presumably resulting from the high work of fracture of the interface and the nearly Mode II deformation of this configuration, and from the vanishing strain energy of the thermal shock cracks.

(iii) No plastic deformation is discernible in the metallic interlayers after thermal shock loading. This fact accords well with the limited opening of the crack in thermally shocked ceramics

(iv) No interaction between the cracking mechanisms in an individual layer and in its adjacent layers takes place. All support the assumption that the cracking mechanisms during thermal shock are localized in an individual layer within the laminate and occur only if sufficient driving forces (stresses) for cracking exist.

(v) Plastic deformation of the NiCu interlayers is another feature of the laminated system. It aims at increasing the work of fracture or, alternatively, the R-curve behavior of the material system.

The advantage of the laminated system over monolithic ceramics under thermal shock conditions was well demonstrated in this investigation. By altering the damage mechanisms to occur in an individual layers without interaction with the damage mechanisms of adjacent layers, the residual strength is derived from the presence of undamaged layers, which is always to be expected due to the nature of the temperature field, and hence the stress field, in thermal shock problems. The residual strength temperature maps, shown in this investigation, exhibit the advantage of the laminated system over the monolithic ceramics. Adapting the design principles drawn in this investigation, using other constituents may lead to further improvement of the residual strength after thermal shock. Finally, we postulate that the behavior under thermal shock cycles may not alter much the damage for a single cycle tests, since damage saturates after few cycles.

Acknowledgement –Special thanks are due to Dr. Rob S. Fredell of the EOARD, and Dr. Allan P. Katz of WPAFB.

	E	ν	σ_Y	σ_{UTS}	α	k	ρ
	GPa	-	MPa	MPa	$^oC^{-1}$	W/(m*K)	g/cm^3
ADS96R	320	.21	-	-	$8.5 \cdot 10^{-6}$	22	3.75
Nickel	200	.31	103-207[3]	379-517[3]	$13.4 \cdot 10^{-6}$	91	8.91
Copper	130	.34	-	-	$16.5 \cdot 10^{-6}$	400	8.92
NiCu[1]	188.3	.315	193-345[4]	483-586[4]	$13.92 \cdot 10^{-6}$	142.6	8.91
NiCu[2]	193.6	.313	193-345[4]	483-586[4]	$13.68 \cdot 10^{-6}$	119	8.91

Table 1. The constituents of the ceramic/metal laminates and their mechanical and thermal properties. [1]83.3% nickel/16.7%copper, [2]90.9% nickel/9.1% copper; properties obtained by 'rule of mixtures'. [3]Properties of Nickel 200, 99.5 Ni, and [4]properties of Monel 400, 66.5 Ni, 31.5 Cu [Metals Handbook, 1985].

REFERENCES

1) D. Sherman and D. Schlumm, J. Mat. Res., 14, 3544-3551 (1999).

2) Z. Chen, J.J. Mecholsky, J. Am. Ceram. Soc., 76, 1258-64 (1993).

3) Z. Chen, J.J. Mecholsky, J. Mater. Res., 8, 2362-9 (1993).

4) Z. Chen, J.J. Mecholsky, S. Hu, J. Mater. Res., 11, 2035-41 (1996).

5) L. Hehn, C. Zhen, J.J. Mecholsky, C.R. Hubbard, J. Mat. Sci., 30, 1277-82 (1995).

6) K.L. Hwu and B. Derby, Acta Mater., 47, 529-43 (1999).

7) Idem, ibid, 545-63.

8) M.C. Shaw, T.W. Clyne, A.C.F. Cocks, N.A. Fleck, .K. Pateras, J. Mech. Phys. Solids, 44, 801-21 (1996).

9) I.E. Reimanis, B.J. Dalgleish and A.G. Evans, Acta. Metall. 39, 3133 (1991).

10) T.S. Oh, J. Rodel, R.M. Cannon and R.O. Ritchie, Acta Met. 36, 2083 (1988).11)

11) E.D. Case, Y. Kim and W.J. Lee, in NATO ASI Series, ; p. 393, Series E: Applied Sci. Vol. 241, , G. A. Schneider and G. Petzow (edts.), Kluwer Academic Publishers, 1993.

12) S. Sato, I. Imamura, A. Kurumada, K. Kawamata, R. Ishida, R. and H. Awaji, ibid, 253.

13) W.J. Clegg, K. Kendall, N.M. Alford, D. Birchall and T.W. Button, Nature 347, 455 (1990).

14) W.J. Clegg, Acta. Metall. Mater. 40, 3093 (1992).

15) D. Sherman, Unpublished results, 1998.

16) R. John, L.P. Zawada, J.L. Kroupa, J. Am. Ceram. Soc., 82, 161-68 (1999).

17) S.S. Lee, L.P. Zawada, J.M. Stachler, C.A. Folsom, J. Am. Ceram. Soc. 1797-811 (1998).

18) M.L. Shalz, B.J. Dalgleish, Tomsia and A.M. Glaeser, Journal-of-Materials-Science. 28, 1673-84 (1993).

19) M.L. Shalz, B.J. Dalgleish, Tomsia and A.M. Glaeser, Journal-of-Materials-Science. 29, 3200-8 (1994).

20) M.L. Shalz, B.J. Dalgleish, Tomsia, R.M. Cannon and A.M. Glaeser, Journal-of-Materials-Science 29, 3678-90 (1994).

21) M.R. Locatelli, A.P. Tomsia, K. Nakashima, B.J. Dalgleish and A.M. Glaeser, Key-Engineering-Materials, **11-112,** 157-90 (1995).

22) B.J. Dalgleish, A.P. Tomsia, K. Nakashima, M.R. Locatelli and A.M. Glaeser, Scripta-Metallurgica-et-Materialia, 31, 1043-8 (1994).

23) D. Sherman and X. Gong, Submitted, 2000.

24) D. Sherman and D. Schlumm, Scripta Mater. 42, 819-825 (2000).

25) S. Timoshenko, *Journal of the Optical Society of America,* 11, 233-255 (1925).

26) S. Timoshenko, in Strength of Materials, Part II, Van Nostrand Co. Inc., New-York, p. 129, (1954).

27) A. Bagchi, G.E. Lucas, Z. Suo and A.G. Evans, *Journal of Materials Research.* **9**, 1734-41 (1994).

28) J.P. Holman, *Heat Transfer*, 6th Ed., McGraw Hill, New-York, 1986.

29) D. Sherman and D. Schlumm, Submitted, 2000.

30) T.J. Lu and N.A. Fleck, Acta Metall., 46, 4755 (1998).

31) S.S. Manson, *Thermal Stress and Low Cycle Fatigue,* McGraw Hill, New-York, 1966.

32) W.J. Lee, Y. Kim and E.D. Case, J. Mat. Sci. 28, 2079 (1993).

33) H. Wang and R.N. Singh, Int. Mat. Rev., 39, 228 (1994).

34) H.F. Nied, J. Thermal Stresses, 6, 217-229 (1983).

FIGURE CAPTIONS

Fig. 1. The Temperature-Pressure-Environment-Time diagram of the processing cycle of the alumina/CuNi laminates.

Fig. 2. The thermal shock apparatus (a) and schematic presentation of a specimen undergoing thermal shock (b).

Fig. 3. SEM micrograph of the alumina / NiCu interface. The interface replicates the morphology of the unpolished alumina layers.

Fig. 4. Load vs. load point deflection curves of laminates with 55 μm thick metallic interlayers under 3PB, before and after thermal shock from 800 and 1000 ^{O}C (a), and that curves of laminates with 30 μm thick metallic interlayers, before and after thermal shock from 400, 600 and 1000 ^{O}C.

Fig. 5. SEM micrographs of the progressive plastic deformation and crack deflection of the metallic interlayers after cracking under 3PB of the unquenched laminate with 55 μm thick metallic interlayers (a-d), a view of the crack deflection at the alumina/CuNi interface (e) and magnified view of the tip of the delamination.

Fig. 6. Close up view of the fully deformed thin (a and b) and thick (c and d) metallic interlayers. Note that the surface of the metallic interlayers replicates the alumina grain morphology.

Fig. 7. Time-temperature curves of the top and the bottom surfaces (a) and of the top and a point 0.5 mm above the bottom surface (b) of a specimen quenched from 1000^{O}C, and the temperature differences between these point, ΔT.

Fig. 8. The cracking mechanisms in an alumina layer of a specimen quenched from 1000^{O}C (with no mechanical loading): an overall view (a), and progressive magnified views of the alumina/NiCu interface (b to d). Note the absence of plastic deformation and crack deflection.

Fig. 9. SEM micrographs of the progressive plastic deformation and crack deflection of the metallic interlayers after cracking under 3PB of the a laminate with 55 μm thick metallic interlayers quenched from 1000^{O}C (a-e), and a view of the crack deflection at the alumina/NiCu interface (f).

Fig. 10. The normalized mass gain and the approximate oxidation depth as a function of time in both types of alumina/NiCu laminates before and after thermal shock from 800 and from 1000^{O}C. The oxidation is almost at steady state in both unquenched laminates, and at decreasing rate after thermal shock.

Fig. 11. SEM micrographs of the oxide metallic interlayers. A close view which demonstrates the crystallographic nature of the oxide layer containing a brittle transverse crack (a), the same at lower magnification, which demonstrates the equally spaced transverse

cracks in the oxide layer (b), and a view of uncracked (c) and cracked (d) oxide layer near fractured alumina layers.

Fig. 12. Optical photographs of a laminate quenched from $1000^{O}C$: the bottom (quenched) surface (a) demonstrates the classical 2-D cracking mechanisms upon quenching, while the photograph of the top surface (b) demonstrates cracks emanating from the edges of the specimen, due to heat transferring through these edges. SEM micrographs of this specimen show two perpendicular cracks. The narrower one is due to the heat transferring through the bottom surface, the wider one was generated due to heat also transferring from the edges (c and d). Higher magnification of the cracked alumina reveals a single grain that bridges the crack surfaces (e).

Fig. 13. The stresses along the z-axis of a laminate containing 55 μm thick (a) and 30 μm thick (b) metallic interlayers, quenched from $1000^{O}C$. The strength of an individual alumina layer was fixed to be 400 MPa, the zero misfit stresses temperature were $665^{O}C$ (a) and $948^{O}C$ (b). C denotes ceramic layers, and M-metallic interlayers. The analysis predicts that three alumina layers will be fractured in the laminate containing thick metallic interlayers, while only two will fractured in that containing thin metallic interlayers. Note that the metallic interlayers are under compressive stresses (a), but under rather low tensile stresses in the second type (b), resulting from the differences between the zero misfit temperature and the quenching temperature.

Fig. 14. The number of broken alumina layers in laminates containing thick (a) and thin (b) metallic interlayers under three point bending as a function of the applied load, P, and the strength of the alumina layers, σ_{CR}, ranged between 200 to 400 MPa. The numbers indicate the number of broken layers. The bold dashed line corresponds to the undamaged laminate, while the other bold lines correspond to reduced laminates of which the outer surface is a metallic interlayer. The other dashed construction lines describe the experimental results. The effective strength, σ_{eff}, is shown as well.

Fig. 15. The calculated and the experimental room temperature residual strength of the two types of laminates, as a function of the thermal shock temperature. The calculations were performed assuming the strength of the individual alumina layer within the laminates to range between 200 and 400 MPa. The bold solid and dashed lines correspond to the laminates containing 55 and 30 μm NiCu interlayers, respectively. The numbers designate the number of broken alumina layers, and the dash and dots line schematically describes the behavior of monolithic ceramic alumina under thermal shock. The circular and the square symbols designate the experimental results of the laminate with thin and thick metallic interlayers, respectively. Note the step like behavior, which is the result of the architecture of the material and the increased residual strength compared with monolithic alumina. The discrepancy in the strength temperature relationship between the experimental results and the numerical model is presumably caused by the edge effect existing in small specimens.

Fig. 16. The experimental set-up for a laminate heated by heating element to examine the behavior under a high steady state thermal gradient (a), and schematic presentation of the cracked laminate and the points at which temperatures were measured (b).

Fig. 17. The temperature distributions at the measuring points on the surfaces of the monolithic and the laminated specimens.

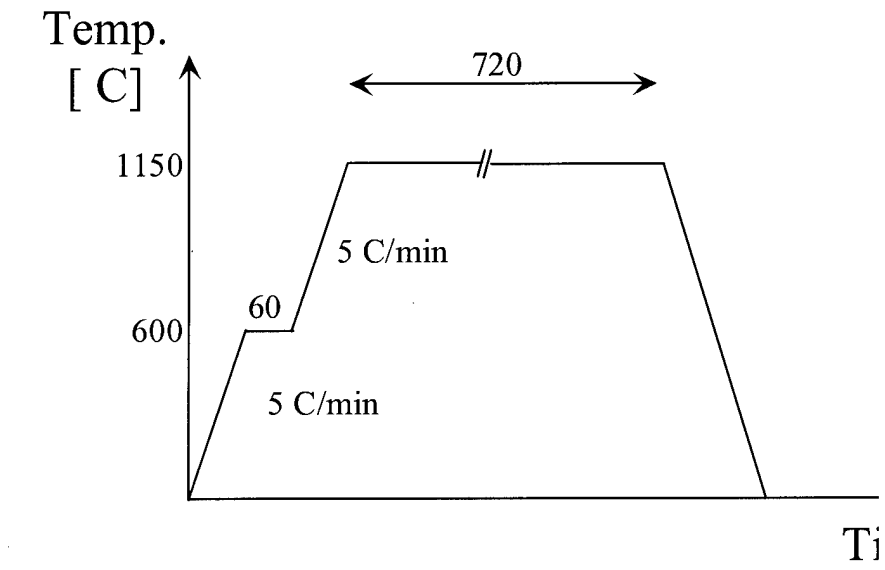

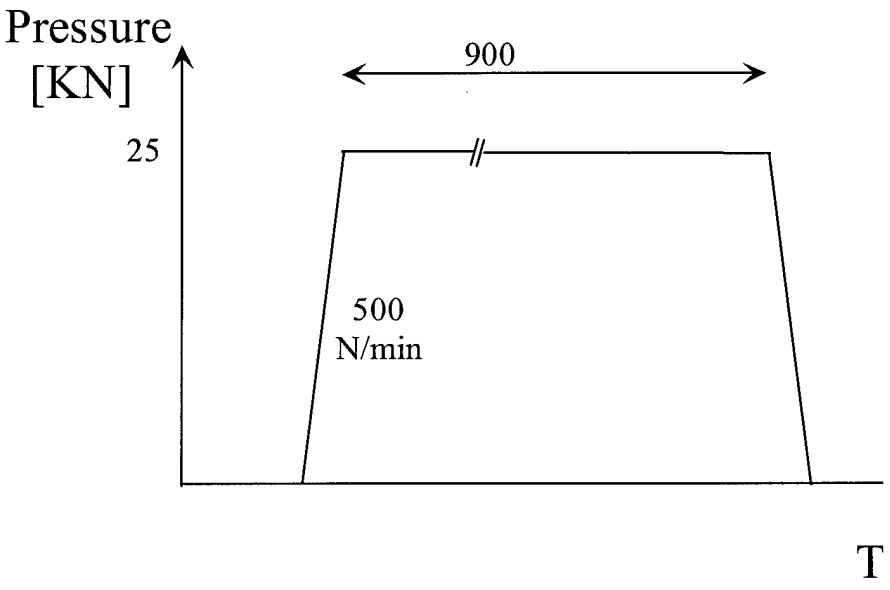

Environment

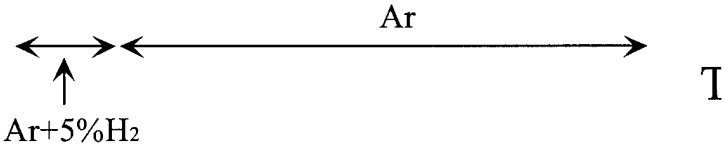

Fig. 1

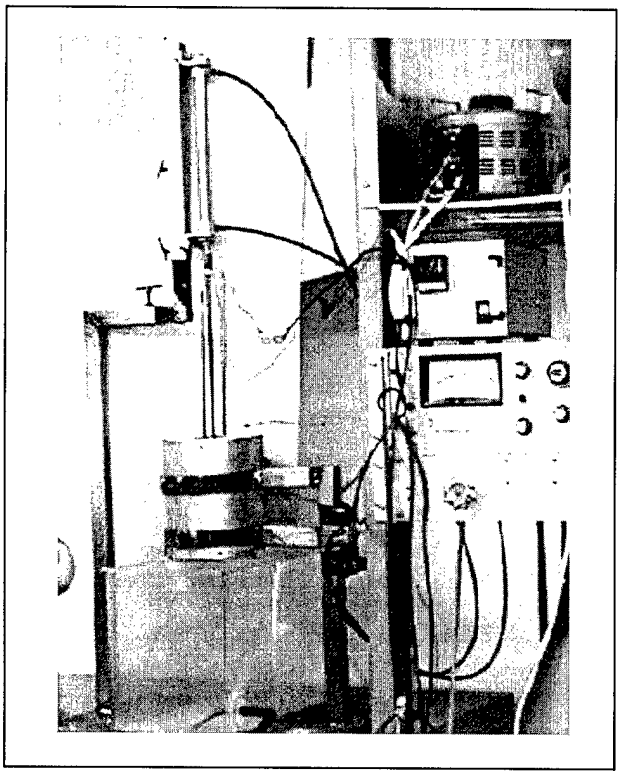

Fig. 2a

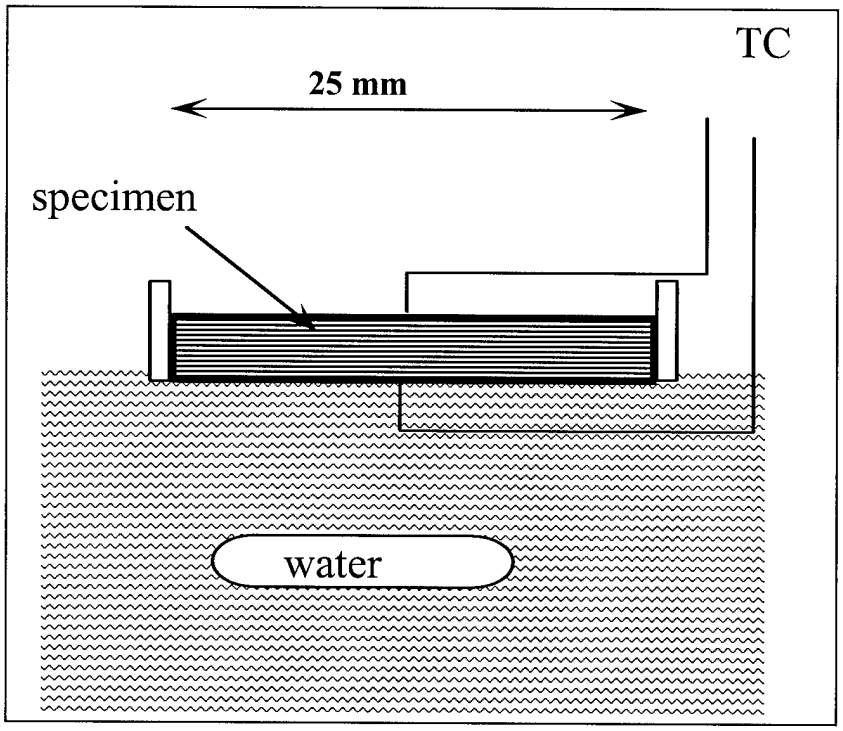

Fig. 2b

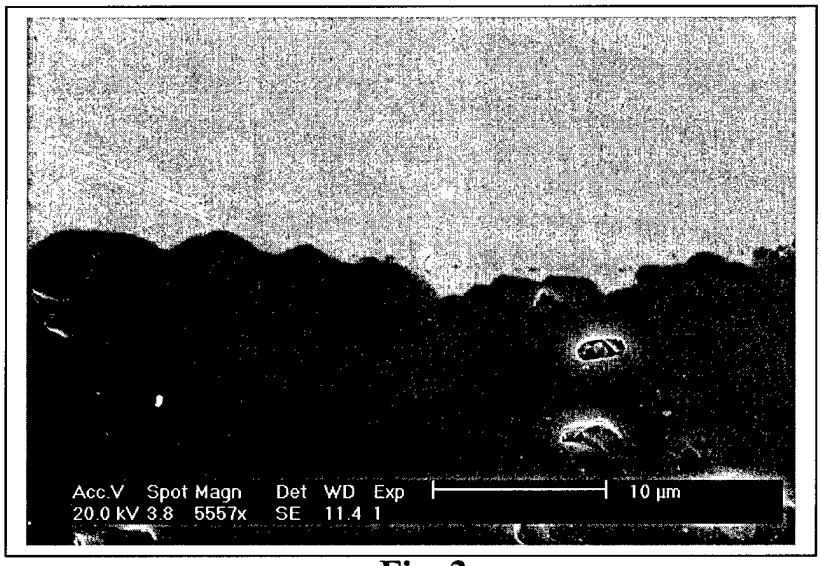

Fig. 3

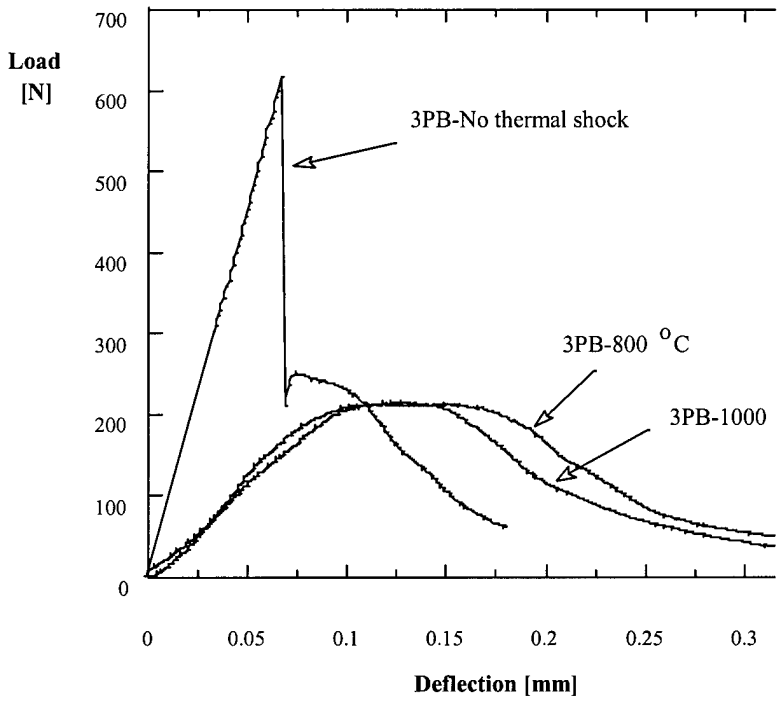

Fig. 4a

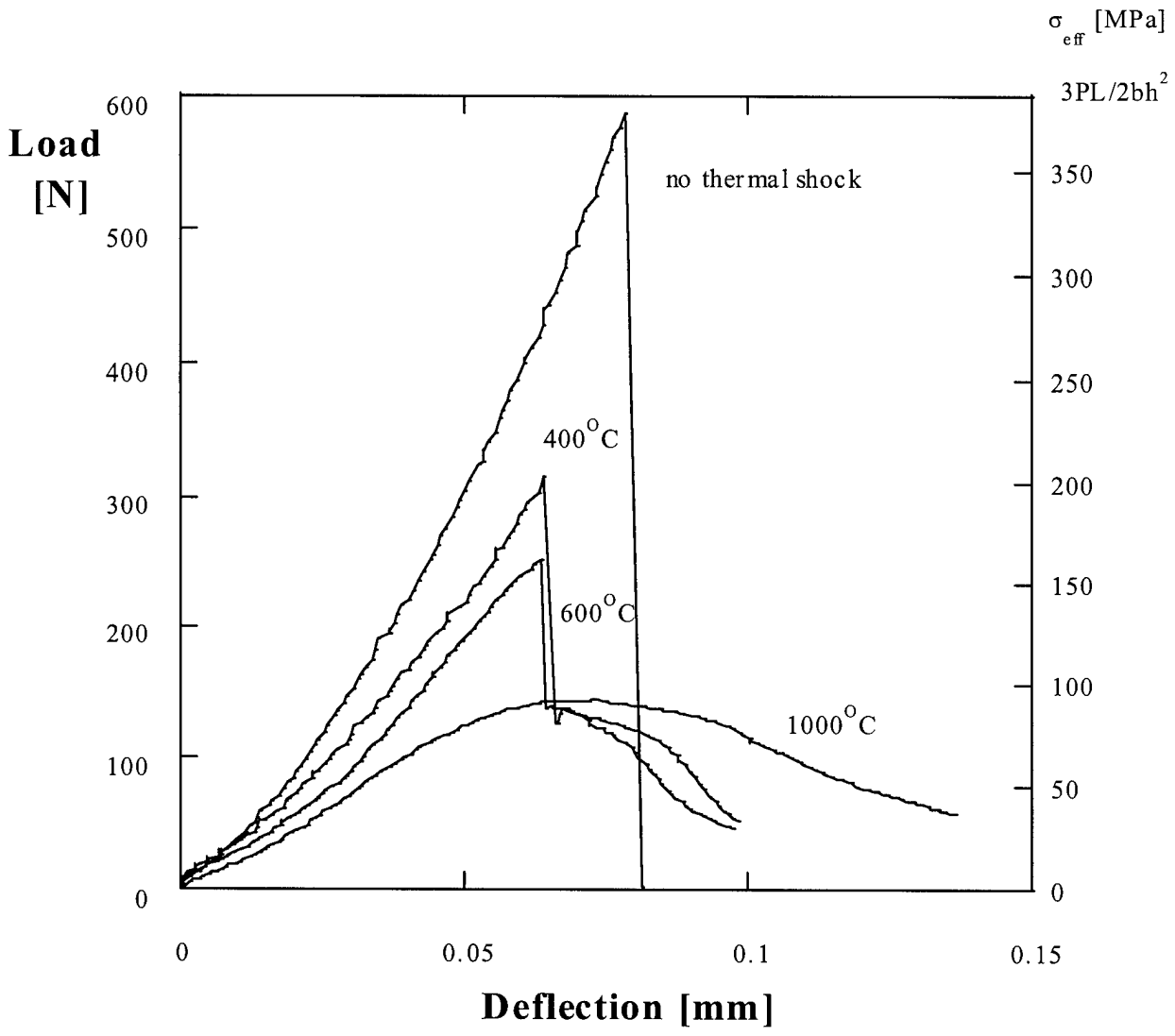
σ eff [MPa]
3PL/2bh²
Load
[N]
600
500
400
300
200
100
0
350
300
250
200
150
100
50
0
no thermal shock
400°C
600°C
1000°C
0
0.05
0.1
0.15
Deflection [mm]

Fig. 4b

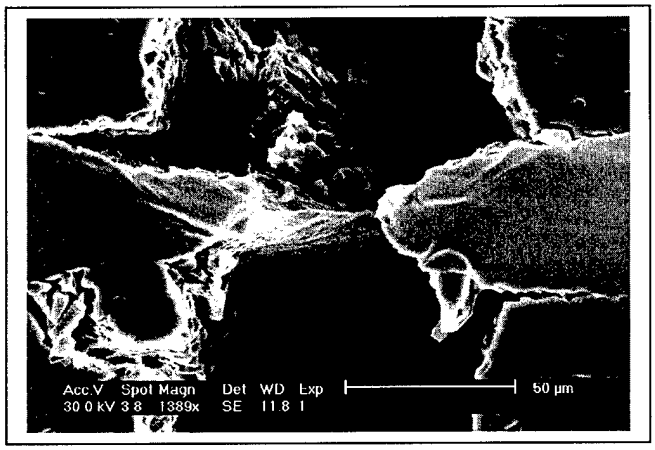

Fig. 5a

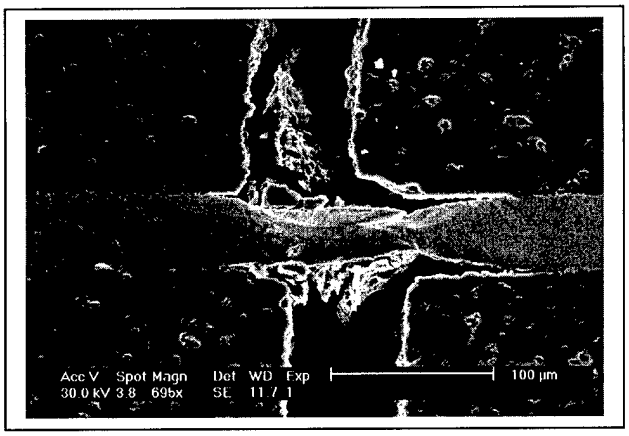

Fig. 5b

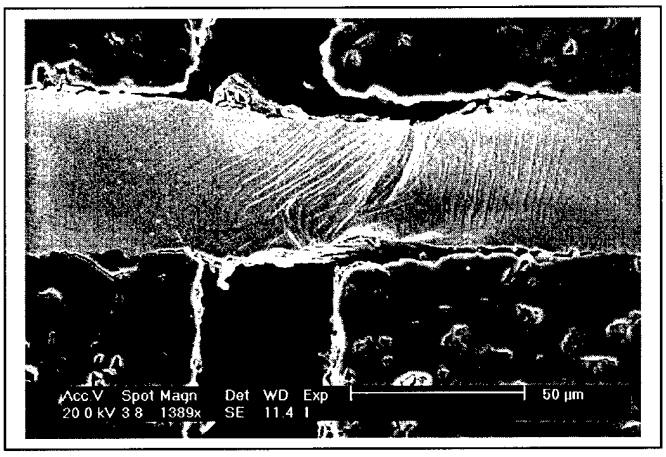

Fig. 5c

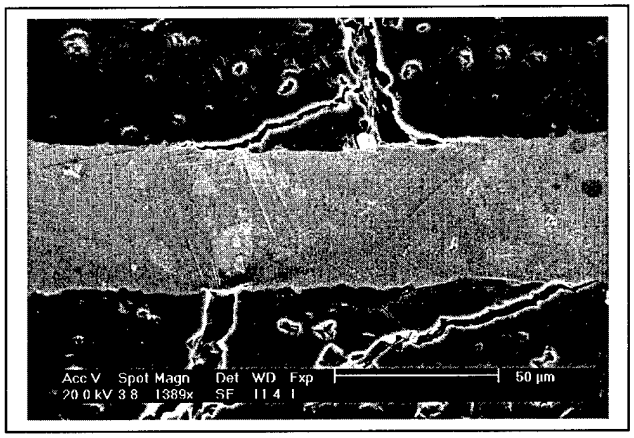

Fig. 5d

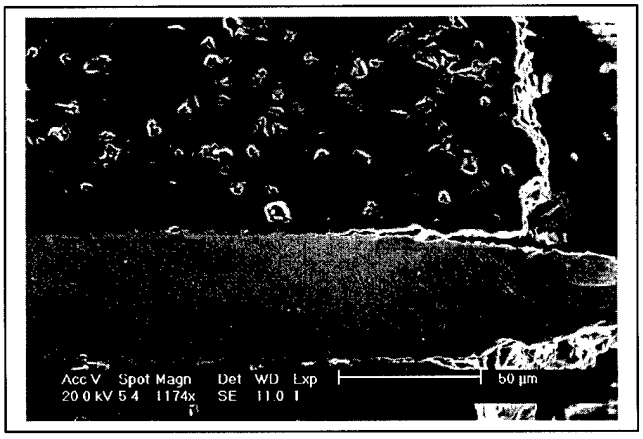

Fig. 5e

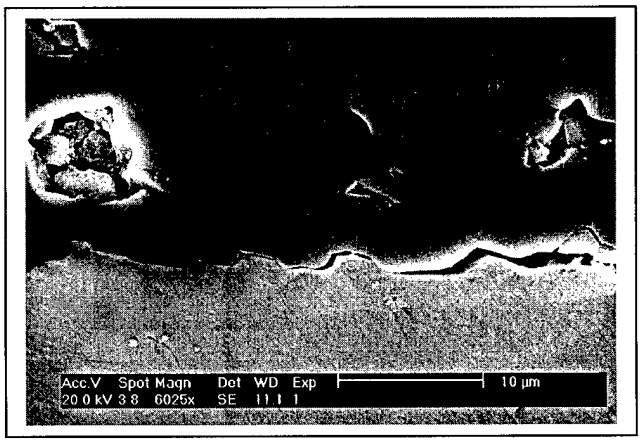

Fig. 5f

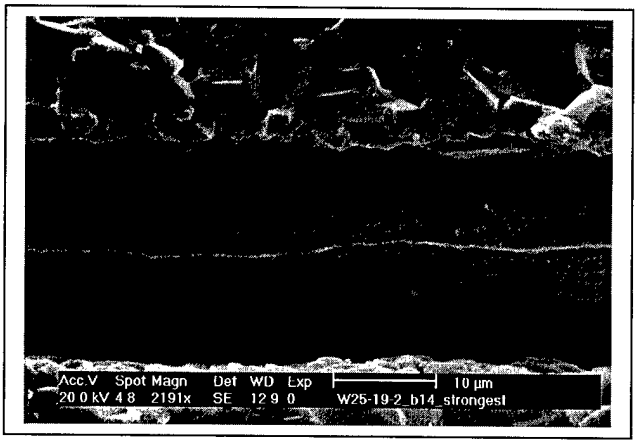

Fig. 6a

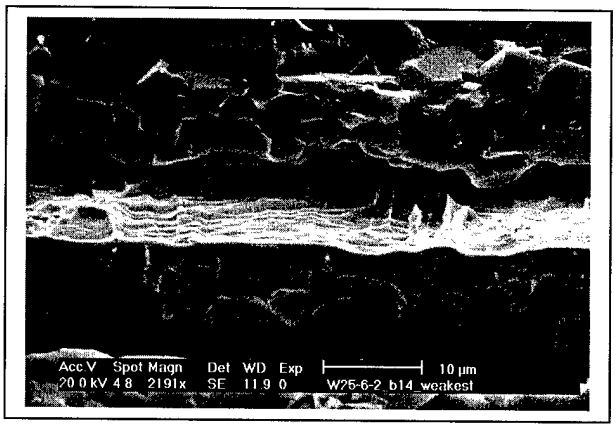

Fig. 6b

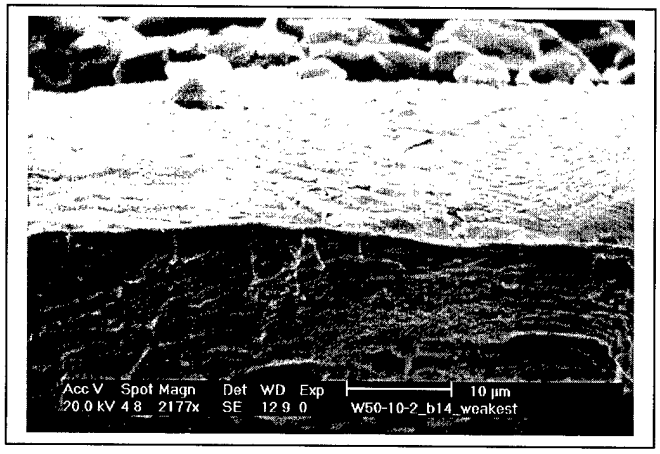

Fig. 6c

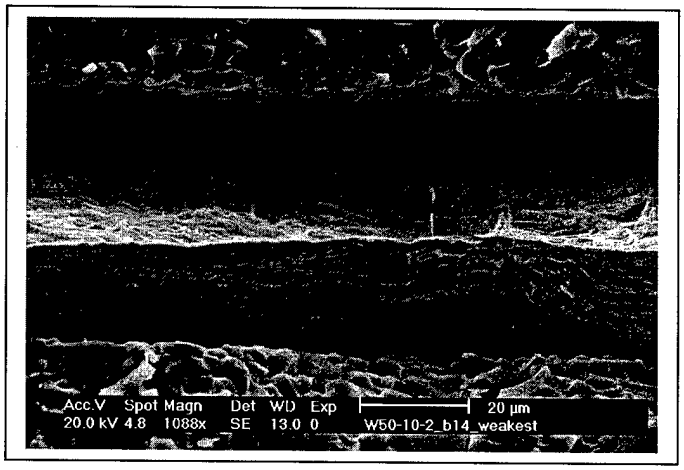

Fig. 6d

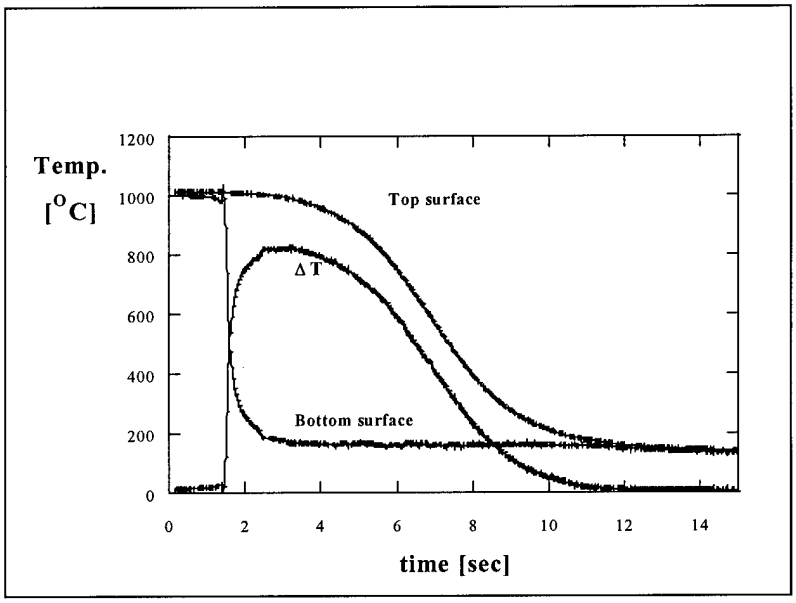
Temp.
[°C]
1200
1000
800
600
400
200
0
Top surface
ΔT
Bottom surface
0
2
4
6
8
10
12
14
time [sec]

Fig. 7a

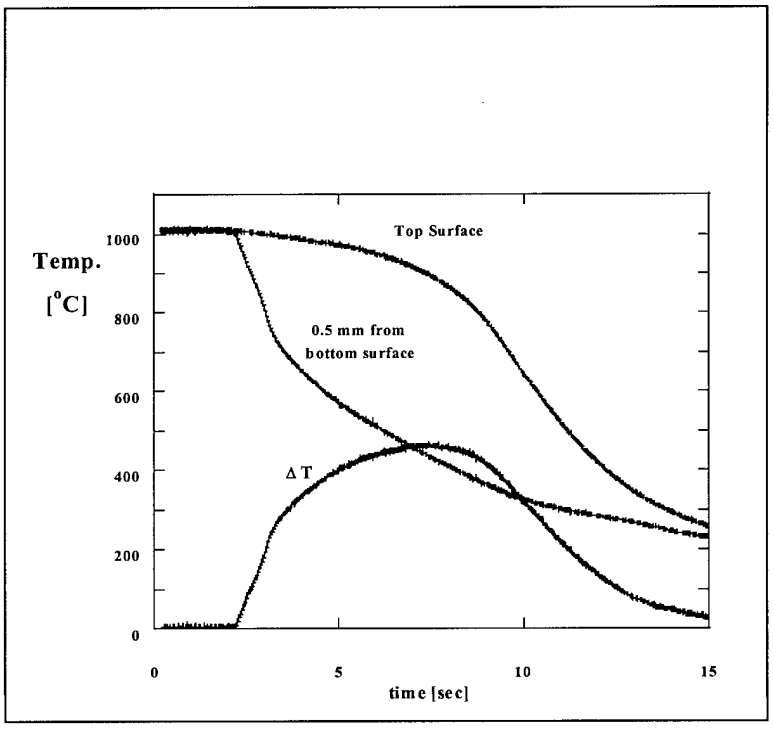
Temp.
[°C]
1000
800
600
400
200
0
Top Surface
0.5 mm from
bottom surface
ΔT
0
5
10
15
time [sec]

Fig. 7b

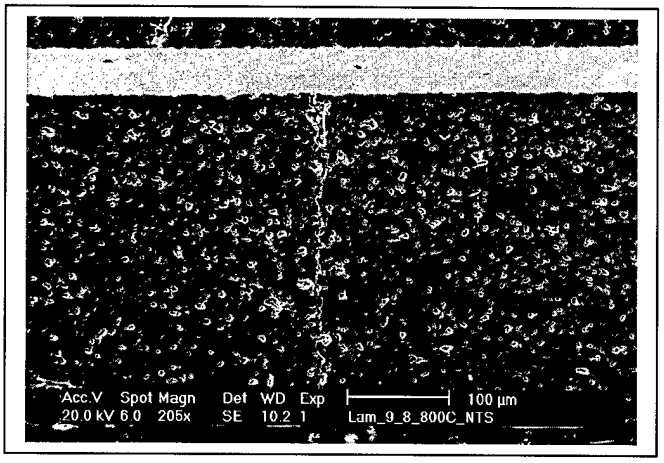

Fig. 8a

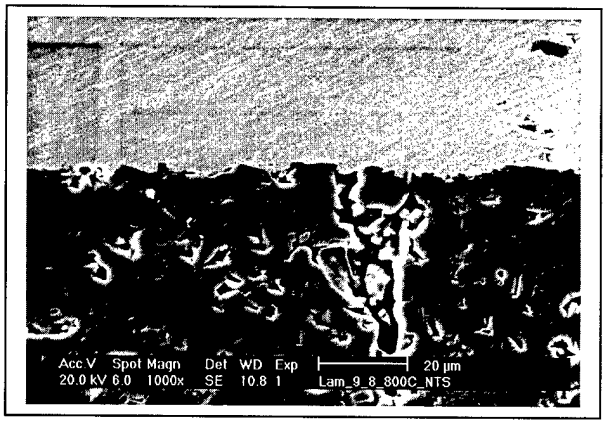

Fig.8b

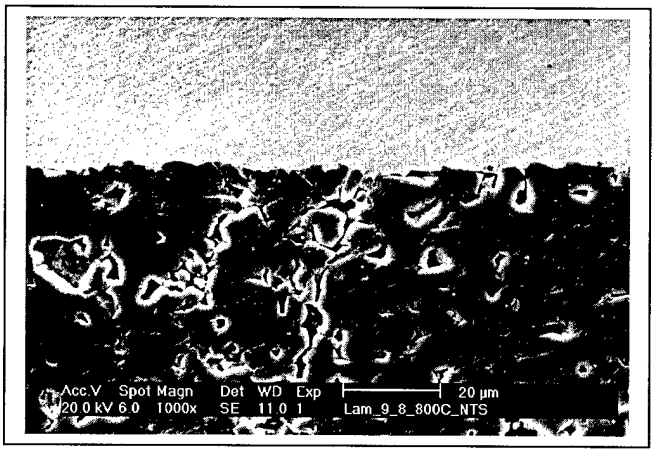

Fig. 8c

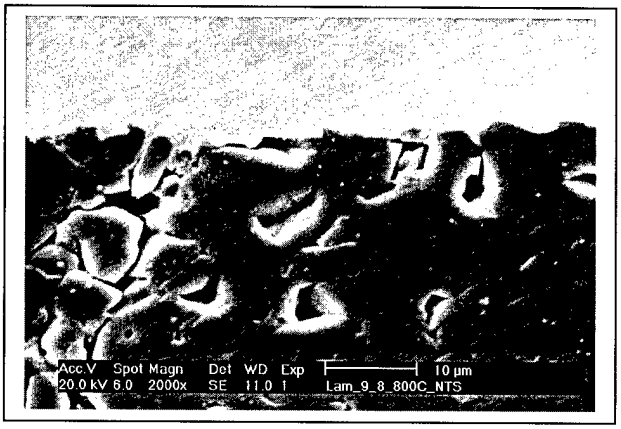

Fig. 8d

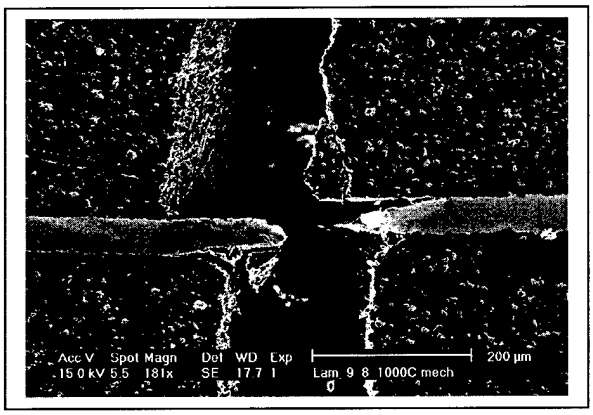

Fig. 9a

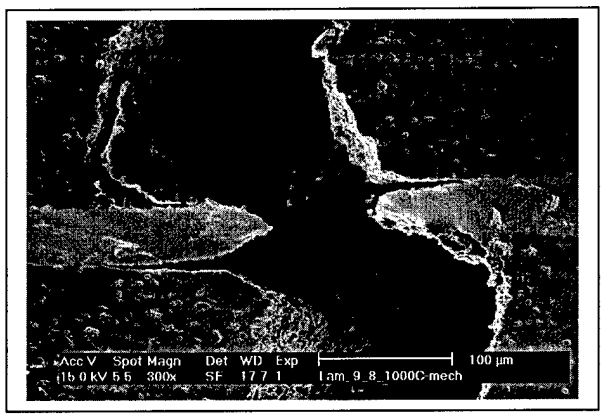

Fig. 9b

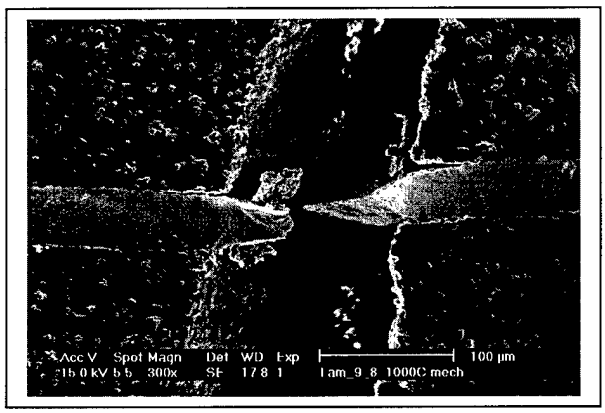

Fig. 9c

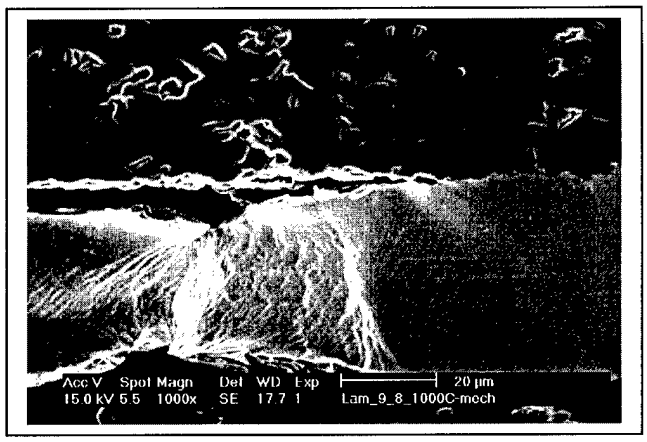

Fig. 9d

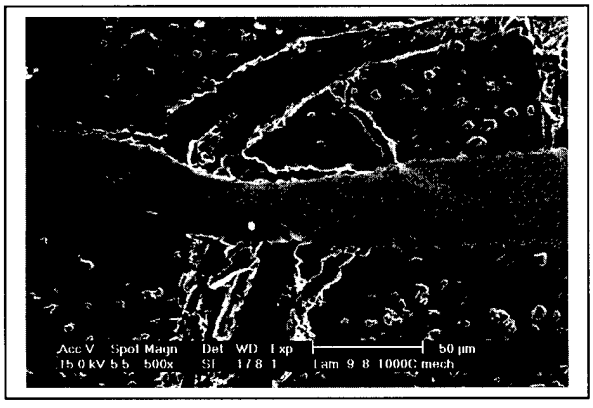

Fig. 9e

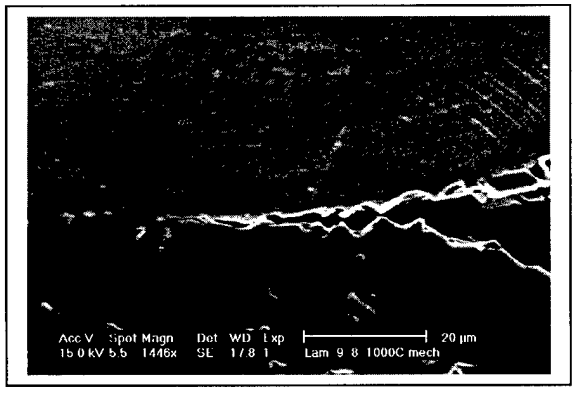

Fig. 9f

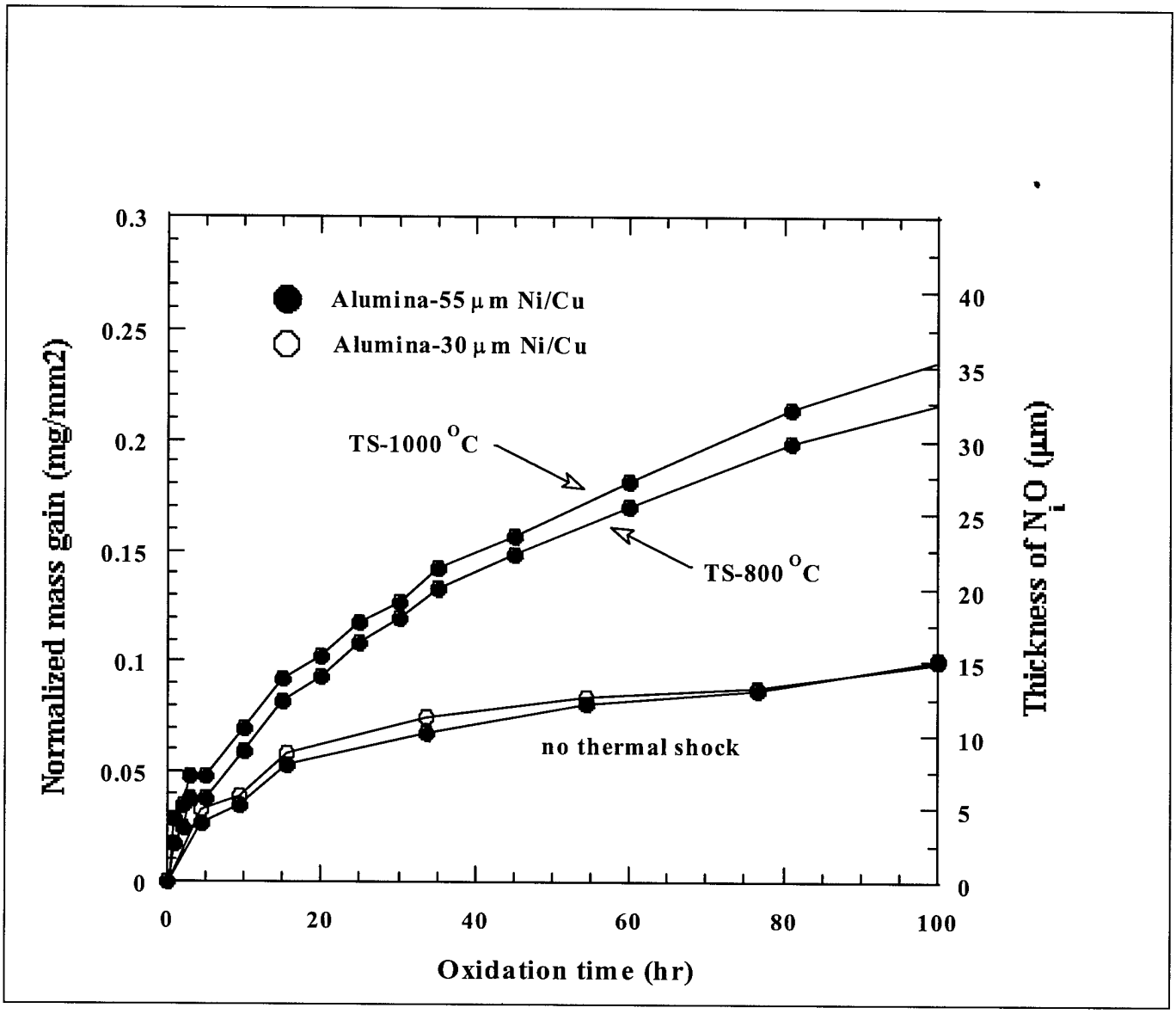
Alumina-55 μm Ni/Cu
Alumina-30 μm Ni/Cu
TS-1000 °C
TS-800 °C
no thermal shock
Normalized mass gain (mg/mm2)
Thickness of NiO (μm)
Oxidation time (hr)
0.3
0.25
0.2
0.15
0.1
0.05
0
40
35
30
25
20
15
10
5
0
0
20
40
60
80
100

Fig. 10

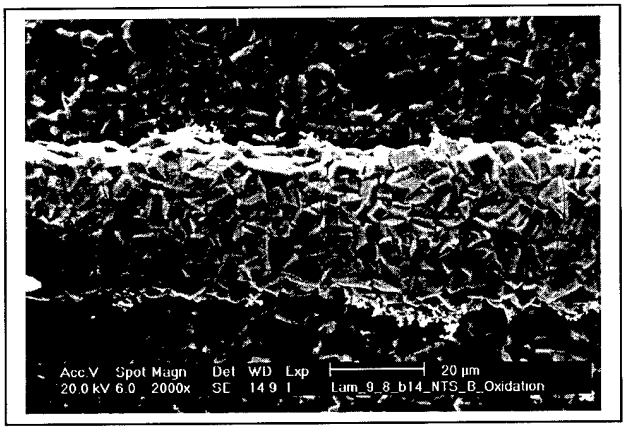

Fig. 11a

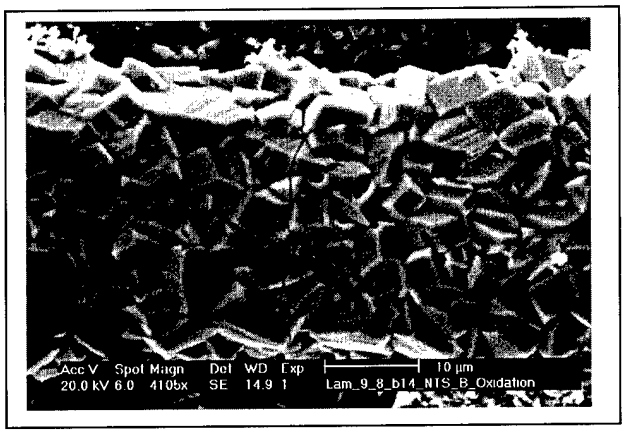

Fig. 11b

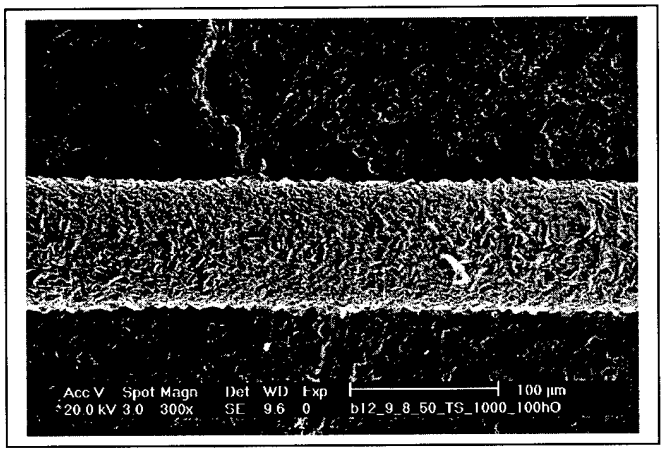

Fig. 11c

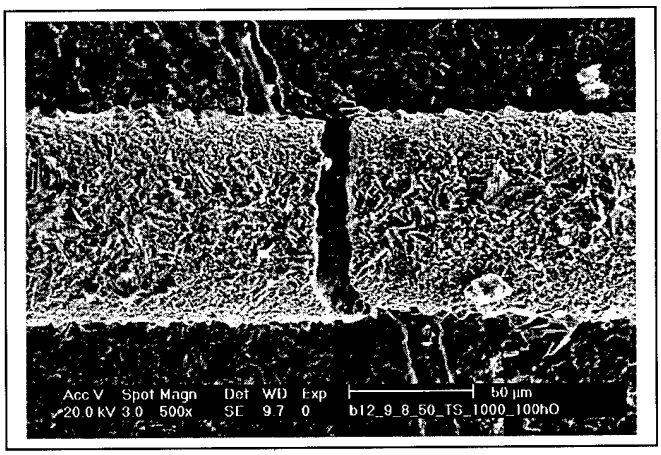

Fig. 11d

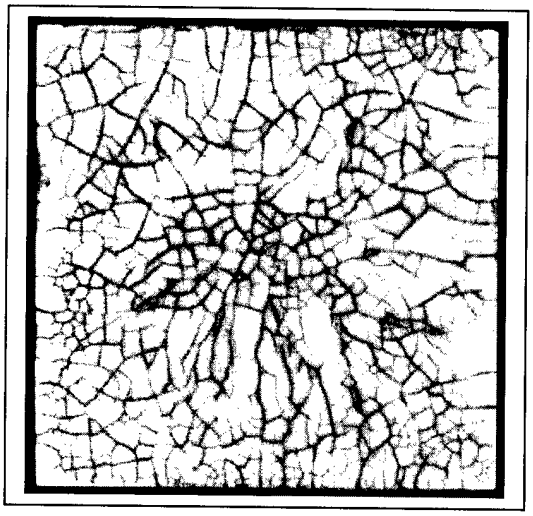

Fig. 12a

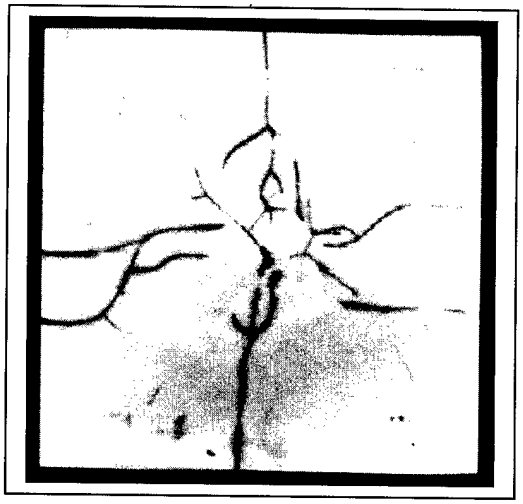

Fig. 12b

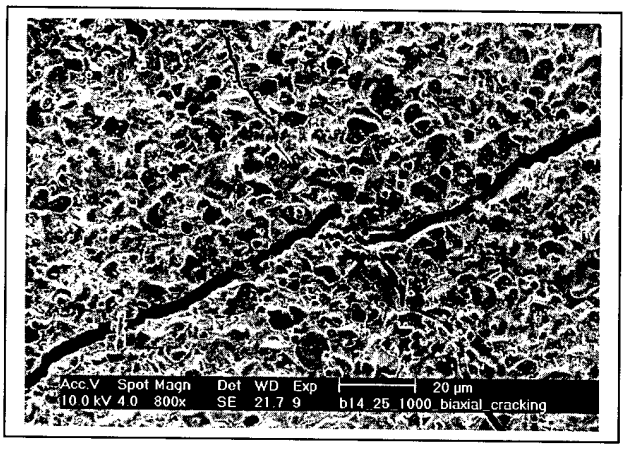

Fig. 12c

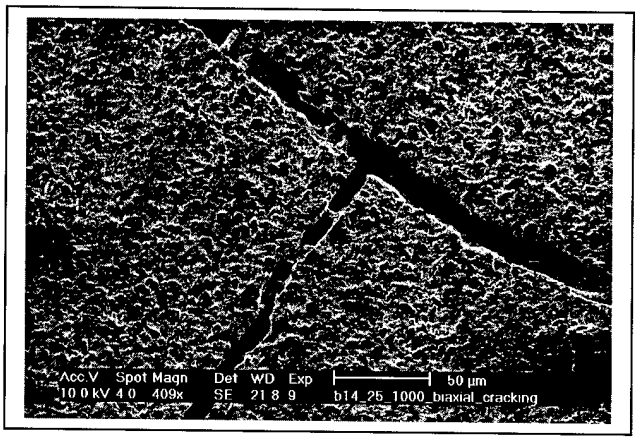

Fig. 12d

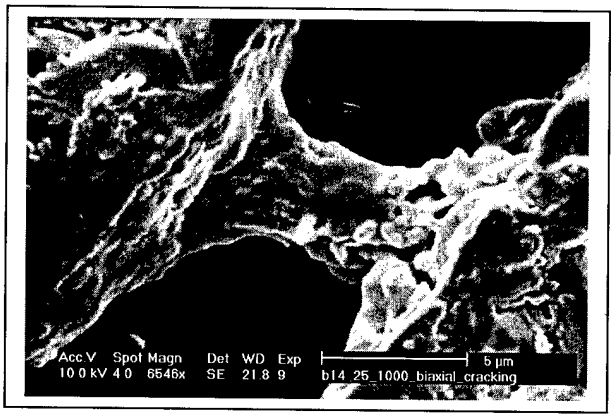

Fig. 12e

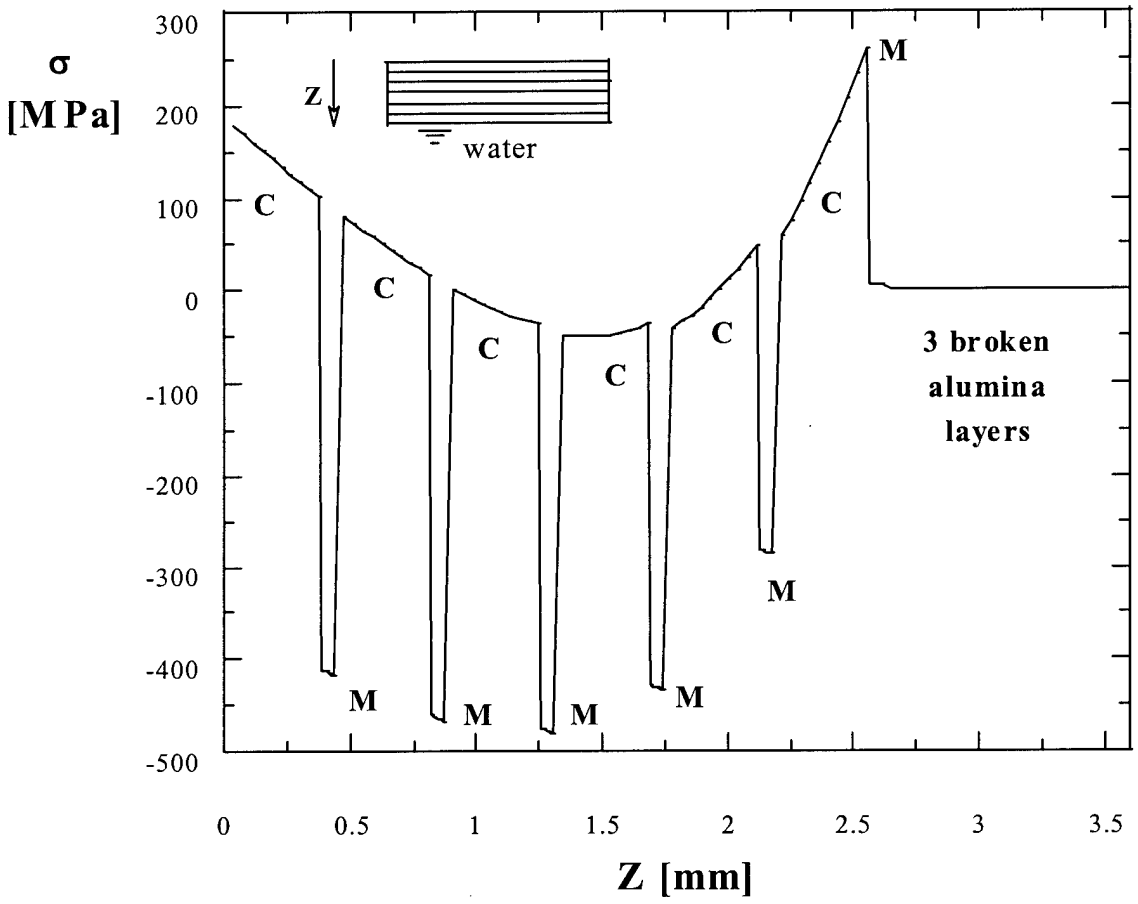
σ
[MPa]
300
200
100
0
-100
-200
-300
-400
-500
Z
water
C
C
C
C
C
C
M
M
M
M
M
M
3 broken
alumina
layers
0
0.5
1
1.5
2
2.5
3
3.5
Z [mm]

Fig. 13a

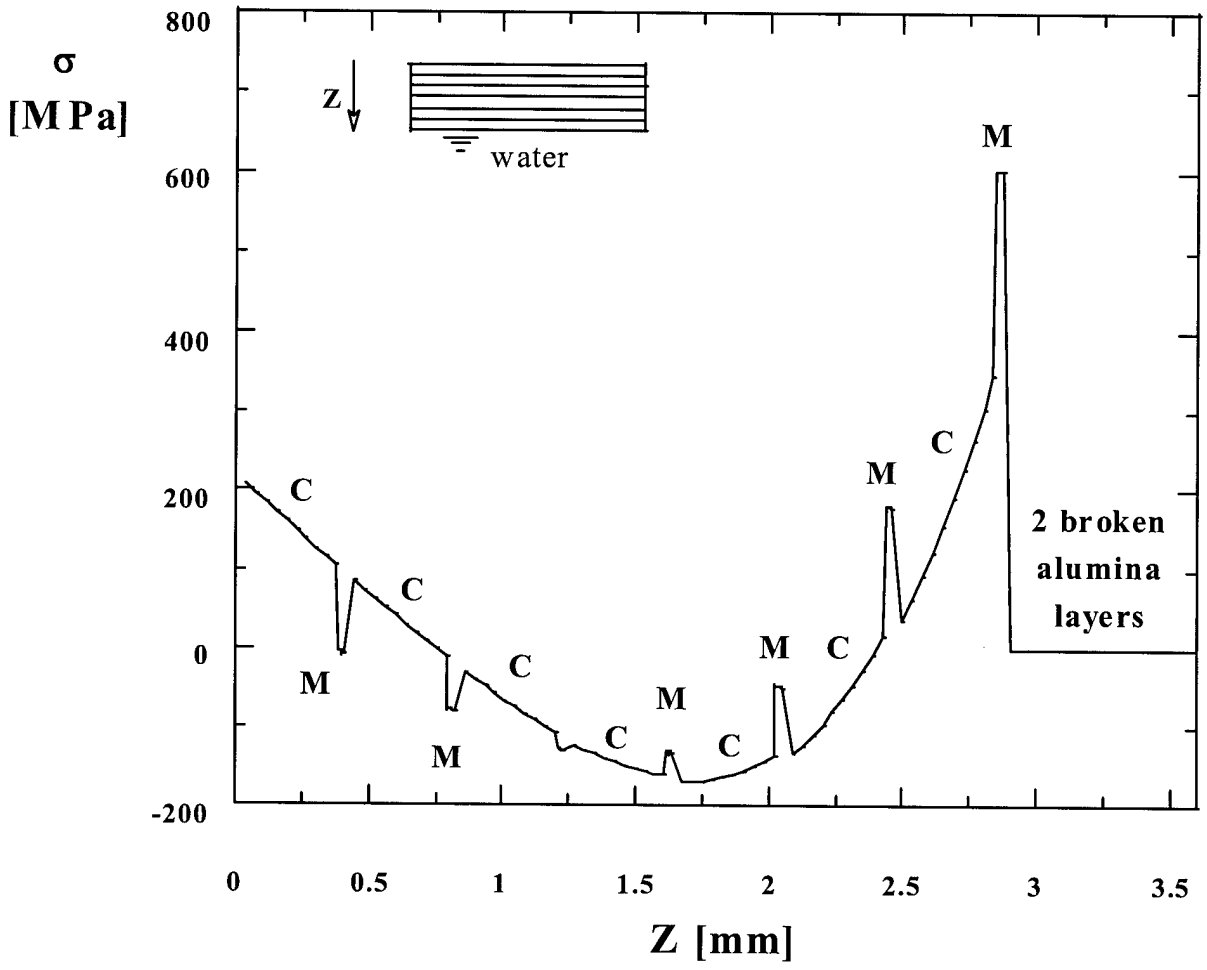
σ
[MPa]
800
600
400
200
0
-200
z
water
C
M
C
M
C
M
C
M
C
M
C
M
2 broken
alumina
layers
0
0.5
1
1.5
2
2.5
3
3.5
Z [mm]

Fig. 13b

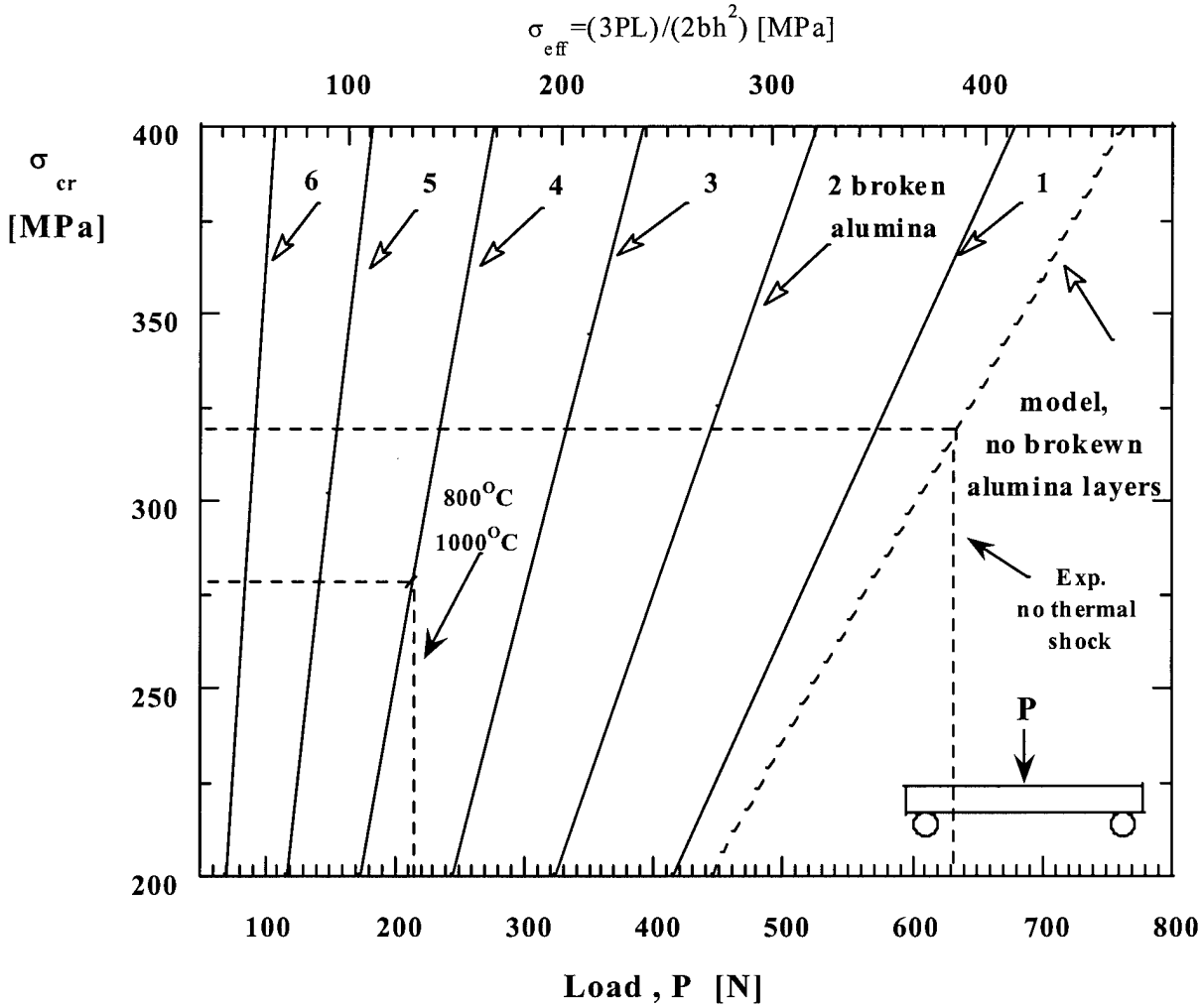
σ eff =(3PL)/(2bh2) [MPa]
100
200
300
400
σ cr
[MPa]
400
350
300
250
200
6
5
4
3
2 broken
alumina
1
model,
no brokewn
alumina layers
800°C
1000°C
Exp.
no thermal
shock
P
100
200
300
400
500
600
700
800
Load , P [N]

Fig. 14a

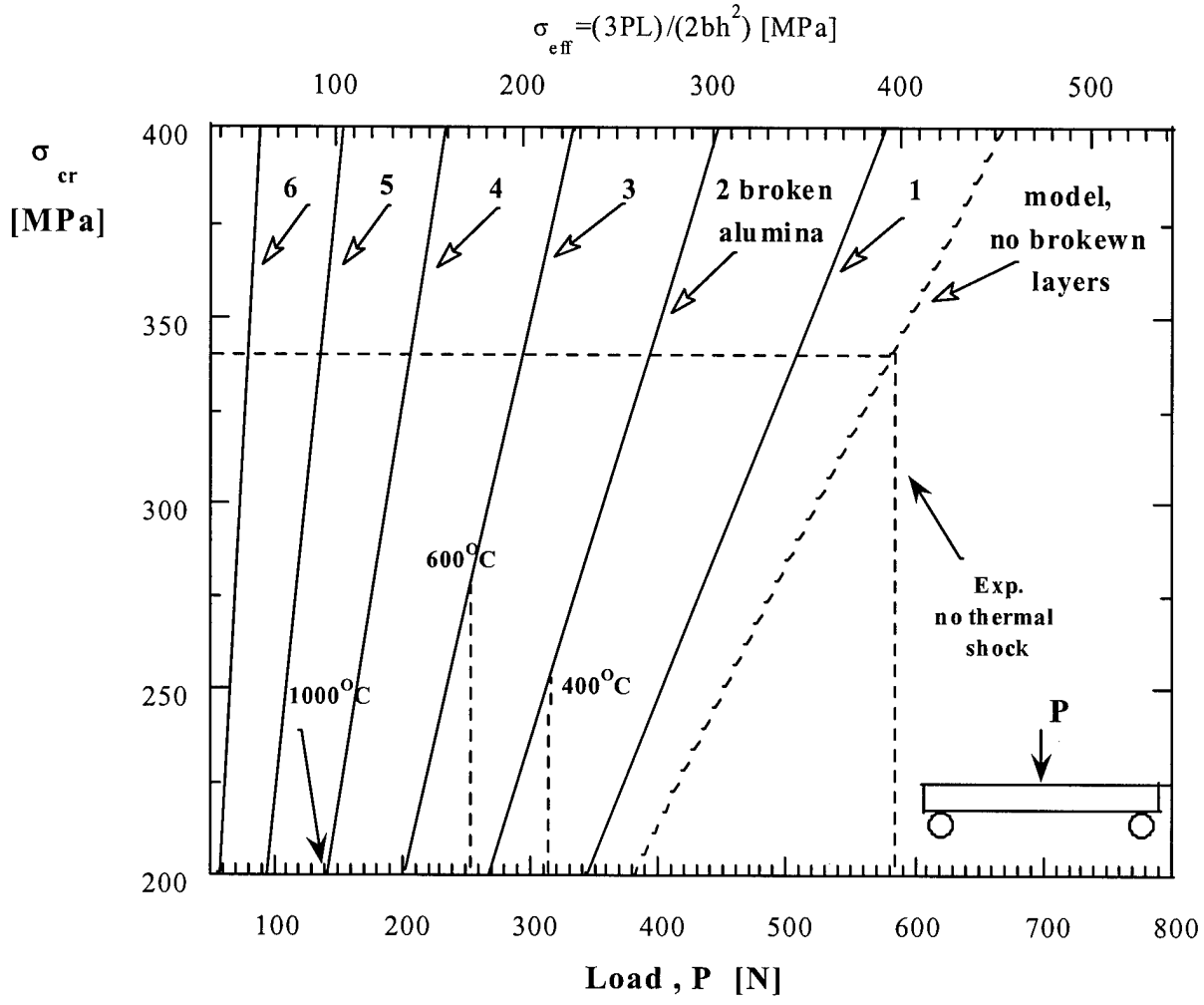
σ eff =(3PL)/(2bh2) [MPa]
100
200
300
400
500
σ cr
[MPa]
400
350
300
250
200
6
5
4
3
2 broken
alumina
1
model,
no brokewn
layers
600°C
1000°C
400°C
Exp.
no thermal
shock
P
100
200
300
400
500
600
700
800
Load , P [N]

Fig. 14b

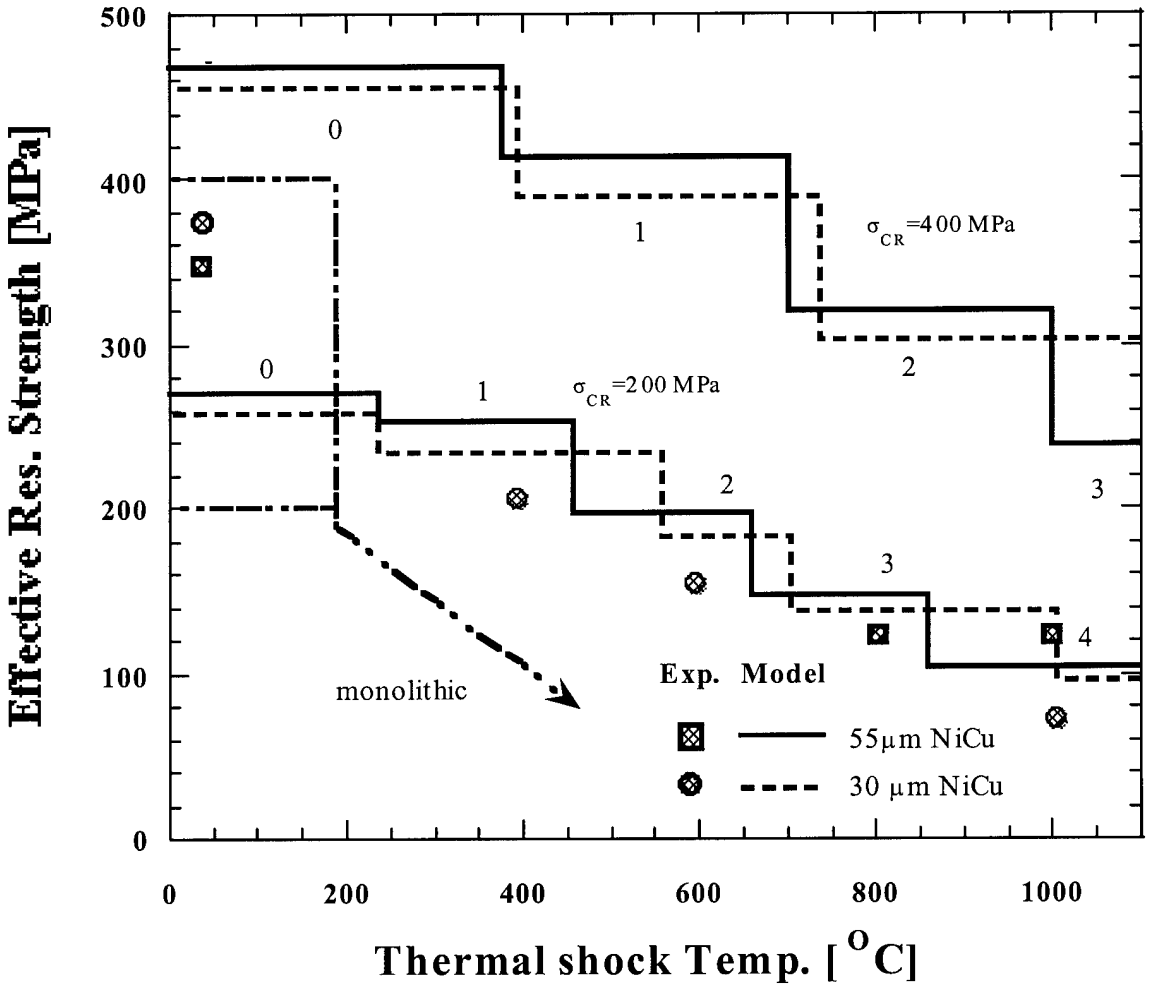
Effective Res. Strength [MPa]
500
400
300
200
100
0
0
200
400
600
800
1000
Thermal shock Temp. [°C]
0
1
2
3
4
σCR=400 MPa
σCR=200 MPa
monolithic
Exp. Model
55μm NiCu
30 μm NiCu

Fig. 15

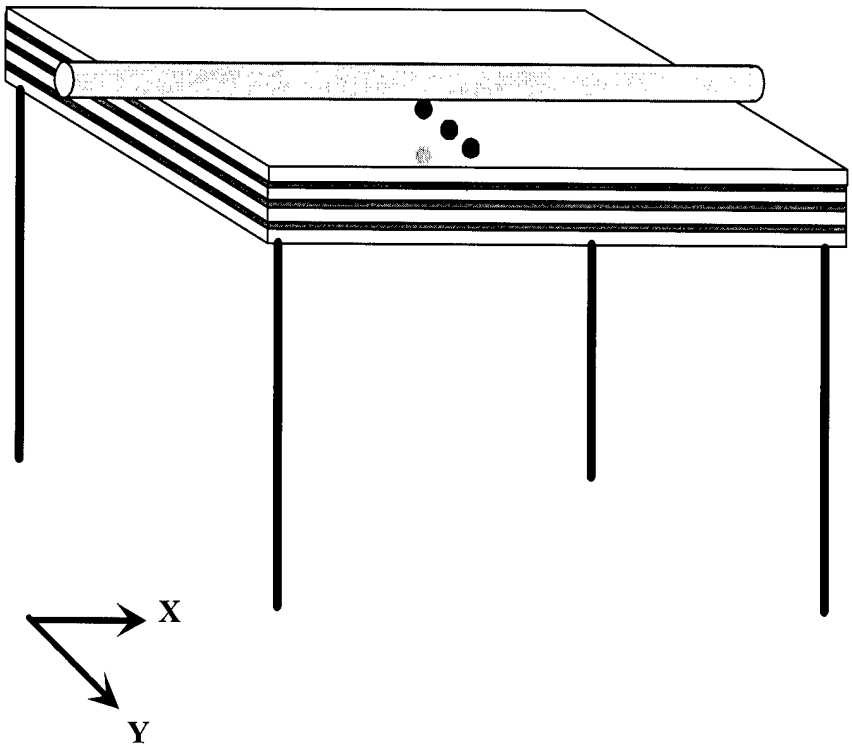

Fig. 16a

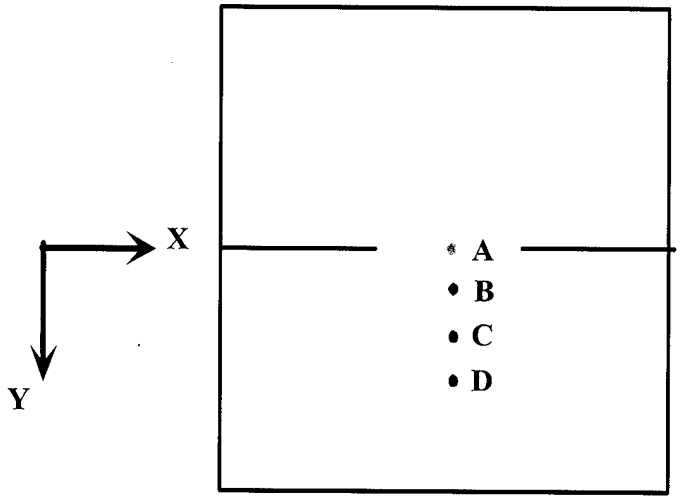

Fig. 16b

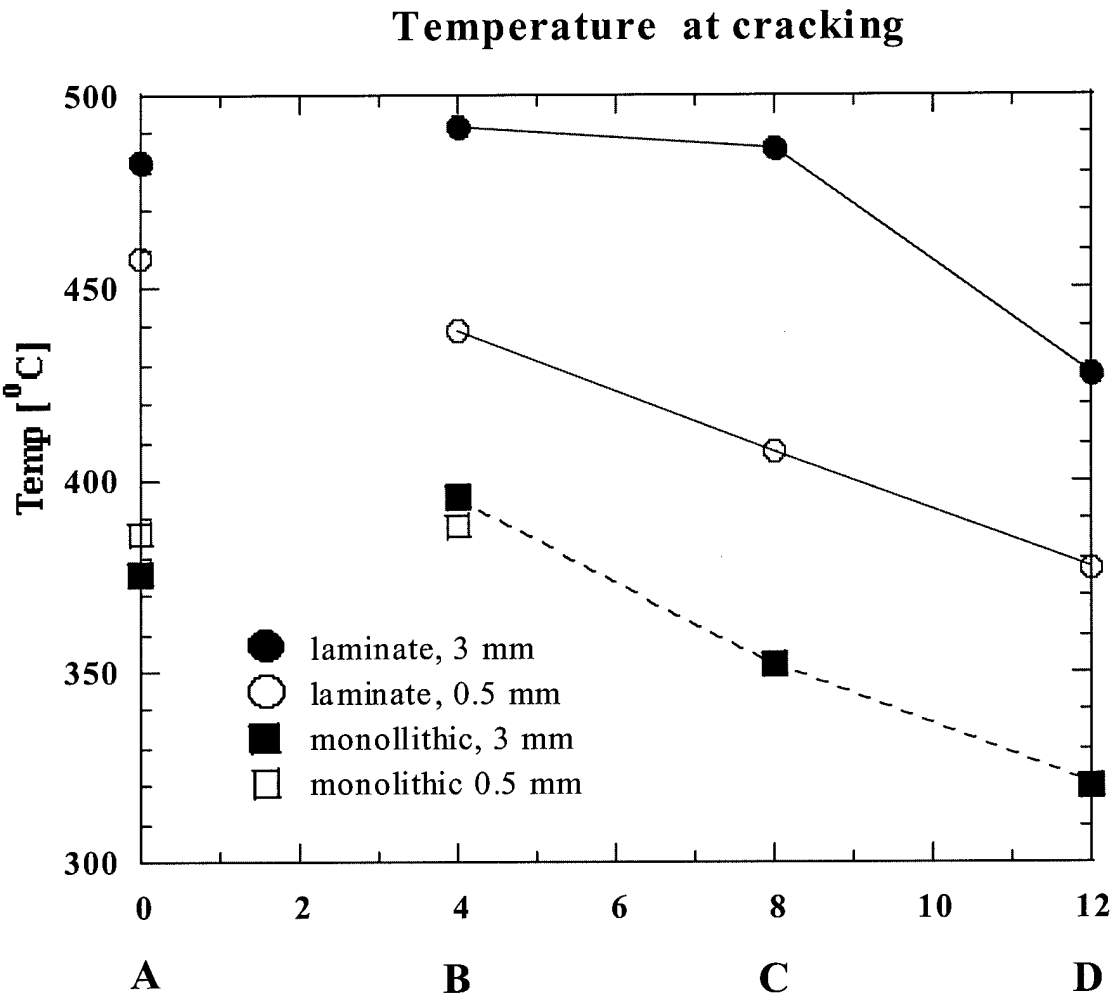
Temperature at cracking
500
450
400
350
300
Temp [^{0}C]
0
2
4
6
8
10
12
A
B
C
D
laminate, 3 mm
laminate, 0.5 mm
monollithic, 3 mm
monolithic 0.5 mm
Location of thermocouple [mm]

Fig. 17

The Statistical Behavior and the Misfit Stresses in Ceramic/metal Laminated System

D. Sherman and X. Gong
Dept. of Materials Engineering
Technion-Israel Institute of Technology
Haifa, 32000 Israel

ABSTRACT

The statistical behavior of ceramic/metal laminates was studied, and in particular the relationship between the failure distribution of the laminate and that of the ceramic layers that it comprises. An important result of this investigation is the ability to predict the misfit stresses due to thermal processing of the laminates.

The failure distributions of an alumina/nickel laminated system and that of the alumina were obtained experimentally by sets of three point bending (3PB) experiments. The relationship between the strength distribution of the alumina in the form of the layers that construct the laminates, and that of the laminated system was established. A finite different scheme was developed, capable of calculating the local stresses at each constituent, and of considering the thermal residual stresses. In addition to the ability to predict the strength of the laminated system by that of the alumina, the thermal residual stresses generated during processing can be evaluated if the strength distribution of the laminate is known.

The laminated system was constructed from 380 μm thick alumina alternating with nickel foil 25 or 50 μm thick. Twenty laminated beam specimens of each type were fractured under 3PB. Thin bending beams made of the alumina layers were also fractured in the same conditions in order to study the statistical behavior of the alumina within the laminated system.

1. INTRODUCTION

The strength distribution of ceramics is the subject of a vast amount of research conducted in the last decades. The pioneering work of Weibull has formulated the probability of ceramics to fail as a cumulative function, known as the 'Two parameters Weibull Statistics': [1]

$$F = 1 - \exp\left[-\int_v \left[\frac{\sigma}{\sigma_0}\right]^m dv\right] \qquad (1)$$

where σ_0 is the median stress and m the Weibull modulus. The main cause of the statistical nature of the strength of ceramics is the distribution, orientation and size of flaws. The statistical nature of beams under bending differs from that of a tensile specimen due to the characteristics of the stressed volume under bending. If a 3PB test piece is loaded, the volume of material subjected to the maximum tensile stress is small, but it is larger for a four point bend (4PB) specimen, while a unidirectional tensile specimen will have the largest volume under maximum stress. It follows that the median strength of a 3PB specimen exceeds that of a 4PB specimen, which in turn should have a higher average strength than a tensile specimen. The measured strength ratio between specimens of identical size subjected to 3PB and to pure tension with same failure probability is predicted to be:[1,2]

$$\frac{\sigma_{3PB}}{\sigma_T} = [2(m+1)^2]^{1/m} \quad (2)$$

which yields 1.73 for m=10, a typical value for a structural ceramic. Clearly, the loading geometry must be considered when comparing the strengths of ceramic components. Assuming uniform stresses in test pieces having different volume but the same failure probability, Weibull statistics predicts a strength ratio:[1]

$$\frac{\sigma_{V1}}{\sigma_{V2}} = \left\lceil \frac{V_2}{V_1} \right\rceil^{1/m} \quad (3)$$

which yields the value of 2 for $V_2=1000V_1$ and m=10, typical for both small test samples and the corresponding large engineering component.

The elastic modulus, the fracture toughness, the density, and the microstructure, by contrast, are not usually sensitive to the size of the engineering components, it being principally the strength that is size-sensitive and is hence not a true material parameter. This has been demonstrated for a commercial glass ceramic[3] and for alumina[4]. It has therefore been suggested that the microstructure and the defect populations themselves may vary throughout the volume of a component, causing variations in strength unpredictable by Weibull analysis[5,6]. An attempt to verify the minimal specimen size required for strength determination was lately made[7].

The current investigation concentrated in the Weibull Statistics of ceramic/metal laminates, and in particular on the correlation between the statistical behavior of the ceramic constituents and that of the laminated system. The statistical distribution of the plastic

deformation was also examined. An important result of this investigation is the ability to predict the thermal residual stresses generated during the joining of the two materials with their distinct coefficients of thermal expansion. This estimation is based on experimental results and a numerical procedure described herein.

2. ANALYSIS

2.1 Statistical analysis

In this section we correlate between the statistical strength distributions of alumina specimens and those of the laminated system, both under three point bending, the alumina specimens and the alumina layers within the laminate are made of same materials and have same geometry.

Consider a beam specimen having b, $2h$, and $2l$ as the width, thickness, and span, respectively. The statistical strength distribution of the material is characterized by the median strength σ_0 and the Weibull Modulus m. The specimen is loaded under 3PB. The risk of rupture assumes the form[1,2]:

$$\int_V \left[\frac{\sigma^B}{\sigma_0}\right]^m dv = \frac{2bhl}{(m+1)^2}\left[\frac{\sigma^B}{\sigma_0}\right]^m \tag{4}$$

In order to calculate the risk of rupture of a laminate, we make the following assumptions: (i) a crack initiates and propagates at the outermost ceramic layer, and that causes the catastrophic failure of the laminate, ii) the coordinates of this layer are z_1 to z_2, where z_1=H, z_2=H-2h, 2H being the total thickness of the laminate and 2h the thickness of an individual layer, the width and the span of the laminate are identical with that of the alumina specimens described above, (iii) the maximum and the minimum tensile stresses in that layer, $\sigma^L_{\max}$ and $\sigma^L_{\min}$, respectively, are known, and (iv) plane stress, and linear elastic behavior is assumed, meaning that no yielding of the metallic interlayers is considered (this subject is discussed below). The tensile stress field in the outermost ceramic layer is formulated as:

$$\sigma^L = \left[\frac{\Delta\sigma}{2h}(z-z_1)+\sigma^L_{\min}\right]\left[1-\frac{x}{l}\right] \tag{5}$$

where $\Delta\sigma=\sigma^L_{\max}-\sigma^L_{\min}$. The risk of rupture of the laminated system is formulated as:

$$\int_V \left(\frac{\sigma^L}{\sigma_0}\right)^m dv = \frac{4bhl}{(m+1)^2}\left[\frac{\left(\sigma^L_{\max}\right)^{m+1} - \left(\sigma^L_{\min}\right)^{m+1}}{\sigma_0^m \Delta\sigma}\right] \tag{6}$$

Assuming same risk of rupture, the relationship between the strength of the ceramic constituent under 3PB and the strength of the laminated system is obtained by equating Eq. (4) and Eq. (6):

$$\left[\sigma^B\right]^m = 2\frac{\left(\sigma^L_{\max}\right)^{m+1} - \left(\sigma^L_{\min}\right)^{m+1}}{\Delta\sigma} \; . \tag{7}$$

For a known failure distribution of the ceramic constituent, the failure probability of the laminate can be validated, provided the stress field in the outermost layer is known. We further formulate this problem using the radius of curvature of the laminate, ρ, and Young's modulus of alumina, E, in order to define the stresses in the outer alumina layer:

$$\sigma^L_{\max} = \frac{E}{\rho}H \tag{8a}$$

$$\sigma^L_{\min} = \frac{E}{\rho}(H - 2h) \tag{8b}$$

Substituting Eqs. (8a) and (8b) into Eq. (7), the relationship becomes:

$$\left[\sigma^B\right]^m = 2(m+1)\left[\frac{E}{\rho}H\right]^m f\left[\frac{2h}{H}, m\right] \tag{9}$$

where:

$$f\left[\frac{2h}{H},m\right]=\left[1-\frac{m}{2}\frac{2h}{H}+\frac{m(m-1)}{6}\left[\frac{2h}{H}\right]^2-\frac{m(m-1)(m-2)}{24}\left[\frac{2h}{H}\right]^3+.....\right]$$

If the strength distribution of the ceramic is known, the predicted maximum stress level in the laminate, $\sigma_{\max}^{L,P}$, is obtained by substituting Eq. (8a) into Eq. (9):

$$\frac{\sigma^B}{\sigma_{\max}^{L,P}}=[2(m+1)]^{1/m}f\left[\frac{2h}{H},m\right]^{1/m}. \quad (10)$$

Eq. (10) can now predict the maximum stresses at the outer alumina layer prior to cracking assuming the misfit stresses in the laminate is zero. With this assumption, Eq. (10) can serve as a design tool to predict the performance of the laminated system under mechanical loading. If the maximum stress in the outer alumina surface, $\sigma_{\max}^{L}$, can be calculated by, say, a certain numerical procedure, a comparison between this stress and the calculated stress, $\sigma_{\max}^{L,P}$, will predict the failure distribution of the laminate and hence the performance or, alternatively, the load carrying capacity of the laminate.

A significant outcome of Eq. (10) is the ability to predict the misfit stresses due to processing, σ_T^L. Assuming that no relaxation of the misfit stress during bending deformation occurs, i.e., elastic behavior of the constituents prevailes, superposition of the thermal stresses into Eq. (10) yields:

$$\frac{\sigma^B}{\sigma_{\max}^{L,E}-\sigma_T^L}=[2(m+1)]^{1/m}f\left[\frac{2h}{H},m\right]^{1/m} \quad (11)$$

where $\sigma_{\max}^{L,E}$ is the distribution of the maximal tensile stresses in the outer alumina layers at cracking, calculated by a numerical procedure using the *experimental failure loads* and assuming zero misfit stresses at, say, room temperature or the temperature at bending. If both the failure distribution of the alumina and that of the laminate are known, the misfit stresses are readily obtained by substituting Eq. (10) into Eq. (11, yielding:

$$\sigma_T^L=\sigma_{\max}^{L,P}-\sigma_{\max}^{L,E} \quad (12a)$$

The final estimation of σ_T^L can be made by using the median stresses of the failure distribution of only the alumina and that of the laminate:

$$\sigma_T^L = \sigma_0{}^{L,P} - \sigma_0{}^{L,E} \tag{12b}$$

In the following section we present the formulae for calculating the stresses in ceramic/metal laminates when subjected to both thermal residual stresses and mechanical loading.

2.2 Calculation of the stresses in a laminate

The statistical analysis requires the calculation of the stresses in the ceramic layers of the laminate in order to correlate between the Weibull Statistics of the alumina under 3PB and the stress field in the outer alumina layer of the laminate, Eqs. (10) and (11). An important parameter to be taken into consideration in that analysis is the thermal residual stresses, σ_T, generated during processing.

The nature of the misfit stresses in ceramic/metal laminated, and in particular in thin metallic interlayers, is complicated. Assuming linear elastic behavior, the misfit stresses obey $\sigma \propto E' \Delta\alpha\Delta T$, where $\Delta\alpha$ is the thermal expansion coefficient mismatch, and $\Delta T = T_R - T$, T_R being the reference temperature at which the misfit stresses are zero. E' is the biaxial modulus. This relationship defines the upper bound for the misfit stresses, usually tensile in the metal interlayers, compressive in the ceramic layers. T_R is not easily defined when ceramic is joined to metal, since deformation mechanisms such as creep may occur at elevated temperatures. A significant complexity arises from the fact that the metallic interlayers are constrained between two ceramic layers, resulting in decreased dislocation mobility, especially at the metal ceramic interface[8]. The thickness ratio of ceramic to metal is another parameter affecting the residual stresses in the metal[9,10], which become elastic as the metallic layers become thinner. For the above reasons, this preliminary study assumes linear elastic behavior of the constituents. This assumption is supported by the experimental results described below; all the load vs. load point deflection relationships prior to the failure of the ceramic layers behaved linearly, which suggested that even at high localized tensile stresses in the metallic interlayers, yielding was

delayed. The bonding between the two adjacent layers is considered to be strong, such that continuity is not violated. The possible formation of product layers is neglected.

The boundary value problem is that of a bending beam subjected to plane stress conditions. The driving force for the stresses are the mismatch of the coefficients of thermal expansion and the external bending moment. The material system consists of n layers, each of an individual thickness, h_n, and of n-1 interfaces.

The stresses in an individual layer are the result of uniformly distributed internal forces, P, which act along the neutral axis of the layer, of internal and external moments, M_i, and M_{ext}, respectively, distributed along the edges of the plates, and the misfit stresses due to processing at high temperatures. The forces and moments equilibrium across the specimen layers dictate[11,12]:

$$\sum_{i=1}^{n} P_i = 0 \tag{13}$$

and

$$\sum_{i=1}^{n} M_i(t) + M_{ext} - \sum_{i=1}^{n-1} P_i(t)\left[\frac{h_i + h_n}{2} + \sum_{k=i+1}^{n-1} h_k\right] = 0 \tag{14}$$

respectively. The analysis assumes a constant radius of curvature of all the layers, such that:

$$M_i = \kappa E_i I_i \tag{15}$$

where $E_i I_i$ is the bending rigidity of the beam. The kinematic assumption in this calculation arises from the strain compatibility across each of the n-1 interfaces, from which:

$$\alpha_i \Delta T_i + \frac{P_i}{E_i h_i} + \frac{h_i \kappa(t)}{2} = \alpha_{i+1} \Delta T_{i+1} + \frac{P_{i+1}}{E_{i+1} h_{i+1}} - \frac{h_{i+1} \kappa}{2}, \tag{16}$$

The problem consists of 2n+1 unknowns (n forces, n moments, and the radius of curvature) and hence of 2n+1 equations, Eqs. (13) to (16)[12]. The incorporate solution is aimed at calculating the internal force vector, P_i. Detailed formulations can be found in Ref. 13. For a known internal force vector, $P_i(t)$, and radius of curvature, $\kappa(t)$, the stresses are:

$$\sigma_i = \frac{P_i}{h_i} + \frac{h_i E_i}{2}\kappa \tag{17}$$

3. EXPERIMENTAL

3.1 Materials

The ceramic layers in this investigation are 2"x2" ADS96R Coor's 96% pure alumina, of 380 μm average thickness. The metallic interlayers are Johnson Matthey Company's 99% pure annealed nickel foils, 25 and 50 μm thick. Nickel was chosen for its relatively high melting point (1453^{O}C), high modulus of elasticity and high strength, the positive mismatch between the thermal expansion coefficients of nickel and alumina, and finally, the relatively simple method of joining it with alumina. The low cost and availability of the 99% pure nickel foils is an additional advantage. The thermal and mechanical properties of the nickel and the alumina are given in **Table 1**.

3.2 Processing

The combined liquid state (active brazing) and solid state (diffusion bonding) was chosen as the joining method[14]. The following processing route was adopted: the alumina layers were coated on both sides by a thin film of 100Å pure Ti, and by a pure copper film of 2.5 μm average thickness on top of the Ti thin film, both deposited by an electron beam sputtering machine. The mechanical and the thermal properties of the copper are also shown in **Table 1**, in addition to the estimated properties of solid solutions of Ni/Cu. No special surface treatment of the alumina layer was applied, aside from cleaning them with Acetone. The laminated systems were constructed by alternating 9 coated alumina plates and 8 (25 or 50 μm thick) nickel foils. Since copper is fully soluble in nickel, and following WDS estimations that demonstrated constant cupper content in the nickel, it was decided to use the 'rule of mixture' in order to calculate the mechanical and thermal properties of the combined Ni/Cu interlayers. These properties, too, are shown in **Table 1**.

The laminates were put in a Thermal Technology Bonding Furnace®. In the first stage, special attention was paid to clean the surfaces of the layers involved. Three flushing cycles were carried out, in each of which a 10^{-3} Tor vacuum was first achieved, followed by a flow of forming gas (Ar+5% H_2). The specimens were kept for an hour in the forming gas environment at 600^{O}C, free of pressure, and with low gas flow to the atmosphere. At the end of this stage, the forming gas was switched to Ar only, and pressure was applied. The joining temperature was raised to 1150^{O}C, and held for 6 hours, with a maximum applied pressure of 10 MPa. That pressure was kept until complete cooling down of the laminated specimens. A detailed description of the processing will be given elsewhere[15].

3.3 Results

Three point bending (3PB) tests of the two types of laminates and of the monolithic thin alumina layers were carried out. The specimens were all of 3.3 mm nominal width. The total thicknesses of the laminates averaged 3.9 and 3.7 mm for the 55 μm and the 30 μm thick Ni/Cu interlayers, respectively. The specimens were put in a specially designed, fully articulated bending bridge, which enables loading of pure 3PB deformation. The point load velocity was 0.05 mm/min. Twenty specimens of each type were tested.

The load vs. load point deflection curves of the strongest and the weakest of the two types of laminates are shown in **Fig. 1**. All the laminates of either type exhibited linear load-deflection relationships prior to the cracking of the alumina layers, which suggests that no plastic deformation took place up to these points. All the laminates containing thin Ni/Cu interlayers underwent brittle fracture, while those with thicker Ni/Cu interlayers exhibited energy dissipating mechanisms due to plastic deformation of the metallic interlayers after fracture of the alumina layers. The ln ln (1/1-F) vs. ln σ of the laminates and the monolithic alumina are shown in **Fig. 2**. In all of these cases the stresses are the effective stresses at fracture, σ_{eff}, calculated assuming monolithic and homogenized specimen, as follows:

$$\sigma_{eff} = 3P(2l)/2b(2h)^2 \tag{18a}$$

where P is the load to fracture of the ceramic layers. The failure probability, F, was calculated by:

$$F = \frac{i-0.3}{N+0.4} \tag{18b}$$

where i is the current specimen number, and N is the total number of specimens[2]. The median strength, σ_o, was selected as the strength at a failure probability of 0.63, where $\sigma/\sigma_o=1$. The Weibull Moduli of the effective strength distribution of both type of laminates are higher than that of the monolithic alumina, while the median strength of the monolithic alumina is higher than the median strengths of either laminate.

4. MONOLITHIC ALUMINA VS. LAMINATE

The mechanical stresses in the outermost alumina layers under 3PB, σ^L_{max}, prior to cracking, according to Eq. (17), in both laminates, and the strength distribution of the monolithic alumina, also under 3PB, are shown in **Fig. 3**. The experimental loads to fracture of the laminates were substituted into the numerical procedure in order to determine the stresses prior to cracking. These stresses, σ^L_{max}, were calculated as if the processing temperature or, alternatively, the zero misfit stress temperature, T_R, are 1150 and 20°C, the first being the actual processing

temperature; the latter - the room temperature, at which no misfit stresses are generated. The median stresses, σ_0, and the Weibull moduli, m, as a function of T_R are shown in **Table 2**. As expected, the strength of the outer alumina layers should be higher in laminates with no misfit stresses, in order to be able to carry the experimental failure loads. On the other hand, if large misfit stresses exist, the mechanical strengths to support the experimental loads are smaller. For fixed experimental failure loads, the Weibull modulus decreases as the misfit stresses increase. The predicted median strengths, $\sigma_{\max}^{L,P}$, Eq. (10), are 329.3 and 330.6 for the laminate with thick and that with thin metallic interlayers, respectively ($\sigma^B/\sigma_{\max}^L$ are 1.258 and 1.253). These values shows that there is practically no difference, since the influence of the ceramic and the metallic layers' thickness ratio in Eq. (10) is limited.

The thermal residual stress in the laminates can be deduced from Table 2, using Eq. 11b. For a beam geometry (plane stress), obtained by the numerical program these stresses were found to be –76.3 and -63 MPa, for the laminate with 55 μm and 30 μm thick Ni/Cu interlayers, respectively. For these residual stresses, the Weibull Moduli coincide with that of the monolithic alumina. The zero misfit temperature, T_R, for these stresses are 665 and 948^{O}C, for the 55 and the 30 μm thick nickel/copper interlayers. It appears that relaxation of the misfit stresses in a constrained thin metallic interlayer is smaller than in a thick one, since plastic deformation in the form of creep is presumably more difficult in thinner constrained layers. The misfit stresses in the alumina layers and in the Ni/Cu interlayers of both laminates at room temperature, using the obtained zero misfit temperature are shown in **Table 3**, for both the plane stress and the biaxial state of stress. Due to Poisson Ratio effect, the stresses are relaxed when being transferred from plate to beam geometry. The stresses for T_R=1150^{O}C are also shown for comparison. We further match the strength of the laminates, predicted by the monolithic alumina according to Eq. (10), to the experimental results of both laminates with thermal residual stresses, Eq. (11). The match is shown in **Fig. 4**. Both the median stresses and the Weibull moduli coincide.

We next examined the maximum tensile stresses generated in the laminates during mechanical loading and by the misfit stresses. The largest tensile stresses develop in the 30 μm Ni/Cu laminates, due to the high thickness ratio. We used the zero misfit temperature for this laminate (T_R=948^{O}C) and the largest applied load in this group of specimens. The stresses generated in this specimen as a function of the Z coordinate is shown in **Fig. 5**. The maximum tensile stress in the outermost metallic interlayer is 1113.7 MPa, as much as twice the approximate strength of a similar alloy, see **Table 1**. The load vs. load point deflection of this specimen, Fig. 1, exhibits a linear relationship prior to cracking of the alumina layers. We postulate that yielding of the metallic interlayers is delayed due to the fact that the layer is being constrained by two alumina layers.

5. SUMMARY

The aim of this investigation was twofold: one was to formulate the relationship between the strength distribution of ceramic plates and that of laminated system containing the characterized

plates, the other to predict the thermal residual stresses generated during the processing of ceramic/metal laminates. The first aim required the characterization of the strength distribution of the ceramic constituent alone, the second also necessitated a program able to calculate the stresses in the laminates, and the experimental strength distribution of the laminates.

The strength distribution of the alumina specimens and that of the laminated system was achieved by loading to fracture 20 specimens of each type. All the specimens exhibited linear behavior of load vs. load point deflection under three point bending, indicating that plastic deformation is delayed in the metallic interlayers prior to the cracking of the alumina layers. While the behavior of the laminates containing thin metallic interlayers was completely brittle, those laminates with thick metallic interlayers demonstrated energy dissipation mechanisms due to plastic deformation of the metallic interlayers after the ceramic layers had fractured.

Using the formulae presented in this investigation, it was found that the thermal residual stresses in the laminates are lower than the maximum stresses predicted by the elastic assumption, which assumes the zero misfit stresses as being those at maximum processing temperature. This result suggests that stress relaxation takes place upon cooling down, and the zero misfit stresses are therefore lower than those at the maximum processing temperature. The thermal residual stresses in the laminates with thin metallic layers are higher than the stresses in the laminates with thick metallic interlayers, and the zero misfit stress temperature is significantly lower in the latter, which suggests that stress relaxation mechanisms are more significant, and last for greater temperature differences in thick metallic interlayers. Furthermore, assuming linear elasticity, it was shown that the superposed, mechanical and thermal, maximum stresses in the thin metallic interlayers significantly exceed the strength of that layers, presumably because these layers are constrained by ceramic layers, which delays plastic deformation mechanisms such as dislocation mobility and hence delays yielding. This effect is more pronounced in the laminates containing thin metallic interlayers.

Acknowledgement – This material is based upon work supported by the European Office of Aerospace Research and Development, Air Force Office of Scientific Research, Air Force Research Laboratory, under Contract No. F61775-99-WE067. Special thanks are due to Dr. Rob S. Fredell of the EOARD, and Dr. Allan P. Katz of WPAFB.

REFERENCES:

1. W. Weibull, *Swed. Ins. Eng. Res.*, Proc., **151**, 1-45 (1939).
2. R. W. Davidge, *Mechanical Behavior of Ceramics*, Cambridge University Press, Cambridge, 1979.
3. D. Lewis, *Am. Ceram. Soc. Bull.*, **61**, 1208-14 (1982).
4. M. J. Hanney, R. Morrell, *Proc. Br. Ceram Soc.*, **1982**, 13 277-90.,
5. D. Lewis III, S.M. Oyler, *J. Am. Ceram. Soc.*, **59**, 289-307 (1976).
6. J. Seidel, N. Claussen, J. Rodel, *J. Europ. Ceram. Soc.*, **15**, 395-404 (1995).
7. T. Lube, M. Manner, *Key Engineering Materials,* **132**, 488-91 (1997).
8. G. Soyez, G. Elssner and M. Ruhle, J. Mat. Sci., **35**, 1087-1096 (2000)
9. A.G. Evans, and J.W. Hutchinson, Acta Metal., **43**, 2507 (1995)
10. A.G. Evans, J.W. Hutchinson and Y. Wei, Acta Mater., **47**, 4093-4113 (1999).
11. Timoshenko, S., *Journal of the Optical Society of America* **11**, 233-255 (1925).
12. Bagchi, A., Lucas, G.E., Suo, Z. and Evans, A.G., *Journal of Materials Research.* **9,** 1734-41 (1994).
13. D. Sherman and D. Schlumm, Submitted, 2000.
14. M.R. Locatelli, A.P. Tomsia, K. Nakashima, B.J. Dalgleish and A.M. Glaeser, Key-Engineering-Materials. **111-112**, 157-90 (1995).
15. D. Sherman, Mechanical Behavior of Alumina/Nickel Laminates under Thermal shock from 1000^{O}C. In progress.
16. Metals Handbook, Desk Addition, Ed. H.E. Boyer, T.L. Gall, American Society of Metals, 1985, p. 15·22.

FIGURE CAPTIONS.

Fig. 1. Load vs. load point deflection curves of the strongest and the weakest specimens of the 55 and the 30 Ni/Cu laminates. Note the linear behavior of the laminates until the cracking of the alumina layers. The laminates containing thin metallic interlayers exhibit brittle fracture, while those with thick metallic interlayers show plastic deformation of those layers after the cracking of the alumina layers in.

Fig. 2. Ln ln [1/(1-F)] vs. ln σ of the two laminates and of the alumina. The stresses are the effective stresses at fracture, σ_{eff}, calculated assuming monolithic and homogenized specimens

Fig. 3. The distribution of the stresses in the outermost alumina layers prior to cracking, σ^{L}_{max}, according to Eq. (16), in both laminates, and the strength distribution of the alumina, all under 3PB. The experimental loads to fracture of the laminates were input to the numerical analysis for the determination of these stresses. The stresses were calculated for $T_R = 1150$ and 20^{O}C.

Fig. 4. Ln ln [1/(1-F)] vs. ln σ of monolithic alumina and the predicted strength distribution of the laminates according to Eq. (10), assuming no misfit stresses (dark symbols). The open symbols denotes the strength distribution, calculated on the basis of the experimental loads, of the laminates containing 55 and 30 μm thick Ni/Cu interlayers where the misfit stresses are –76.3 and -63 MPa, respectively. The Weibull modulus and the median stresses coincide.

Fig. 5. The maximum tensile stresses in the strongest 30 μm thick Ni/Cu laminate that was subjected to mechanical loading under 3PB. The misfit stress was considered. The maximum tensile stress is in the outer metallic interlayer (1113.7 MPa), which exceeds the tensile strength of the metallic interlayers.

	E	ν	σ_Y		σ_{UTS}
		α	k	ρ	
		GPa	-	MPa	
MPa		$^oC^{-1}$	W/(m*K)	g/cm^3	
ADS96R		320	.21	-	
-		$8.5 \cdot 10^{-6}$	22	3.75	
Nickel		200	.31	103-207[3]	379-517[3]
$13.4 \cdot 10^{-6}$		91	8.91		
Copper	130	.34	-	-	
$16.5 \cdot 10^{-6}$	400	8.92			
Nickel-copper[1]	188.3	.315	193-345[4]	483-586[4]	$13.92 \cdot 10^{-6}$ 142.6
8.91					
Nickel-copper[2]	193.6	.313	193-345[4]	483-586[4]	$13.68 \cdot 10^{-6}$ 119
8.91					

Table 1. The constituents of the ceramic/metal laminates and their mechanical and thermal properties. [1]83.3% nickel/16.7%copper, [2]90.9% nickel/9.1% copper; properties obtained by 'rule of mixtures'. [3]Properties of Nickel 200, 99.5 Ni, and [4]properties of Monel 400, 66.5 Ni, 31.5 Cu [16].

T_R			20^oC		1150^oC	
	alumina	laminate[#]	55 μm	30 μm	55 μm	30 μm
σ_o	414.3	329.3, 330.6	405.6	393.6	250.9	299.6
m	9.6	9.6 , 9.6	12.3	11.1	7.5	8.1

Table 2. The median stresses, σ_o, in MPa, and the Weibull moduli, m, of the alumina, [#] of the laminates predicted by Eq. (10), and of the laminates with 55 and 30 mm thick Ni/Cu interlayers. The failure stresses in the laminates were calculated using the failure loads obtained in testing, assuming the misfit temperatures, T_R, to be 1150 and 20^oC.

	Thick (55 μm) metal laminate				Thin (30 μm) metal laminate			
	alumina			alumina	nickel/copper			nickel/copper
T_R	Biaxial	Pl. σ	Pl. σ	Biaxial	Biaxial	Pl. σ	Biaxial	Pl. σ
948	-		-	**-63.0**	-	-91.5	910.0	1320.6
665	-	**-76.3**	-109.9	-	600.7	865.1	-	-
1150	1108.1	-133.6	-192.5	1608.0	1052.4	1515.6	-76.8	-111.4

Table 3. The misfit stresses at room temperature in the alumina layers and in the metallic interlayers of laminates having 55 and 30 μm Ni/Cu interlayers, at the three characteristic zero misfit temperatures, under plane stress conditions and under biaxial state of stresses. The stresses were calculated using the parameters in **Table 1**.

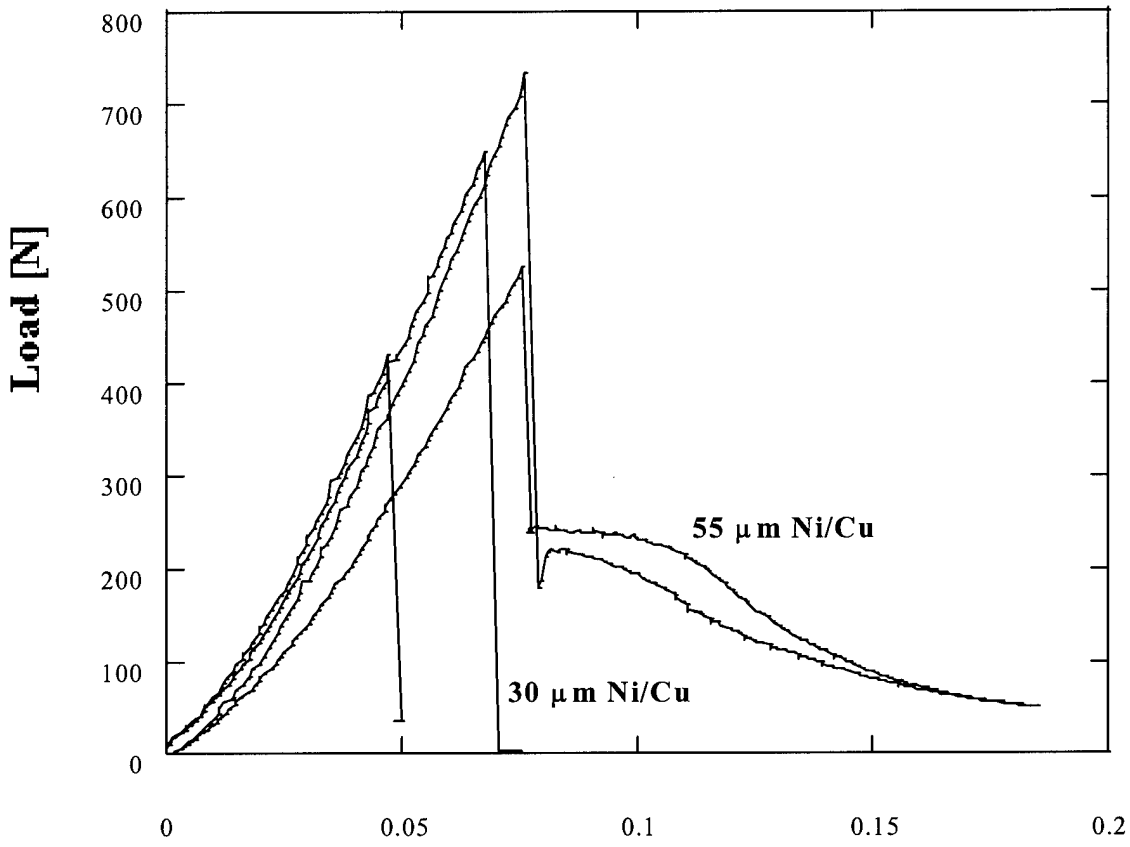
800
700
600
500
400
300
200
100
0
Load [N]
0
0.05
0.1
0.15
0.2
Deflection [mm]
55 μm Ni/Cu
30 μm Ni/Cu

Fig. 1.

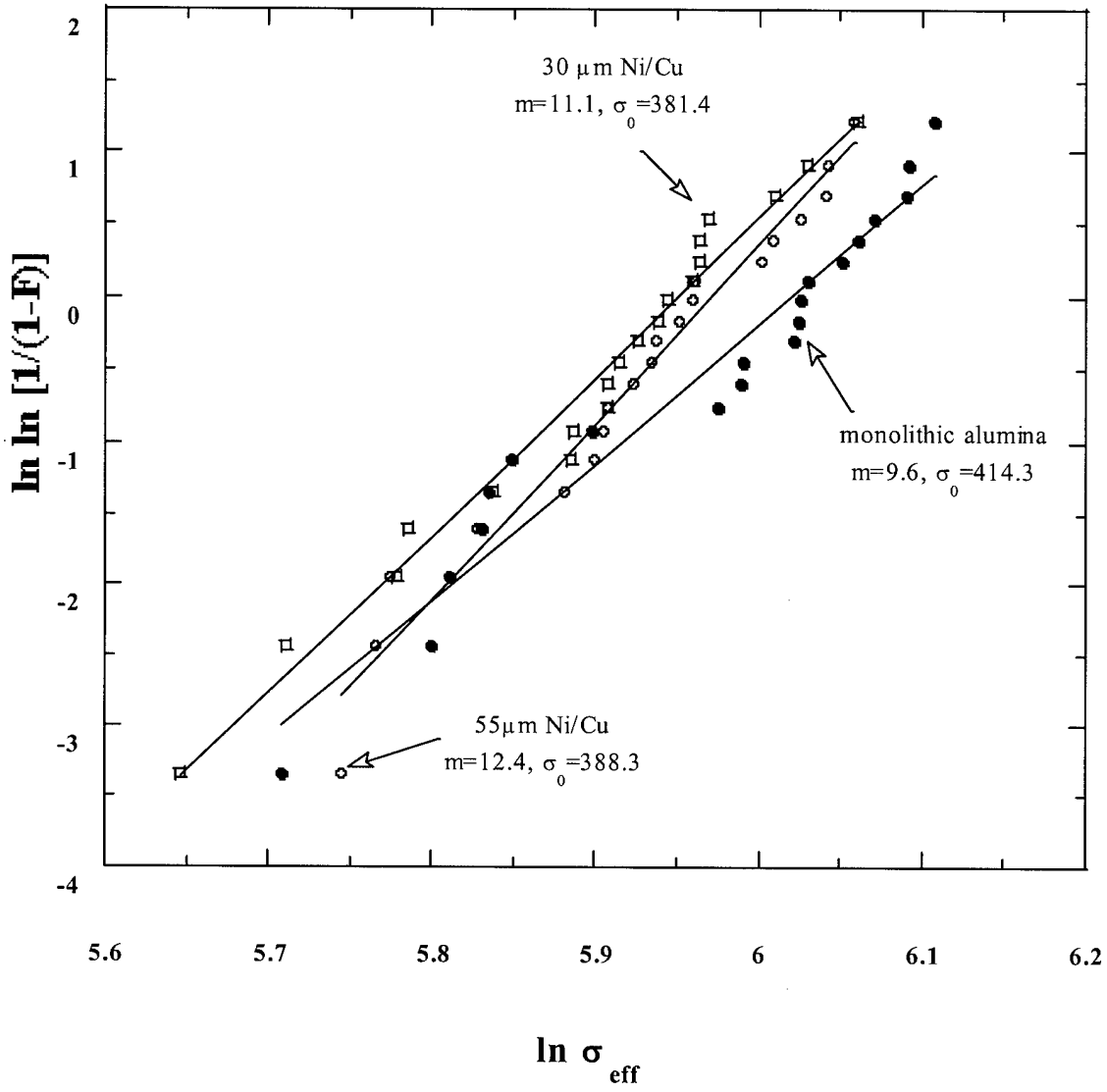
30 μm Ni/Cu
m=11.1, σ0=381.4
monolithic alumina
m=9.6, σ0=414.3
55μm Ni/Cu
m=12.4, σ0=388.3
ln ln [1/(1-F)]
ln σeff
2
1
0
-1
-2
-3
-4
5.6
5.7
5.8
5.9
6
6.1
6.2

Fig. 2

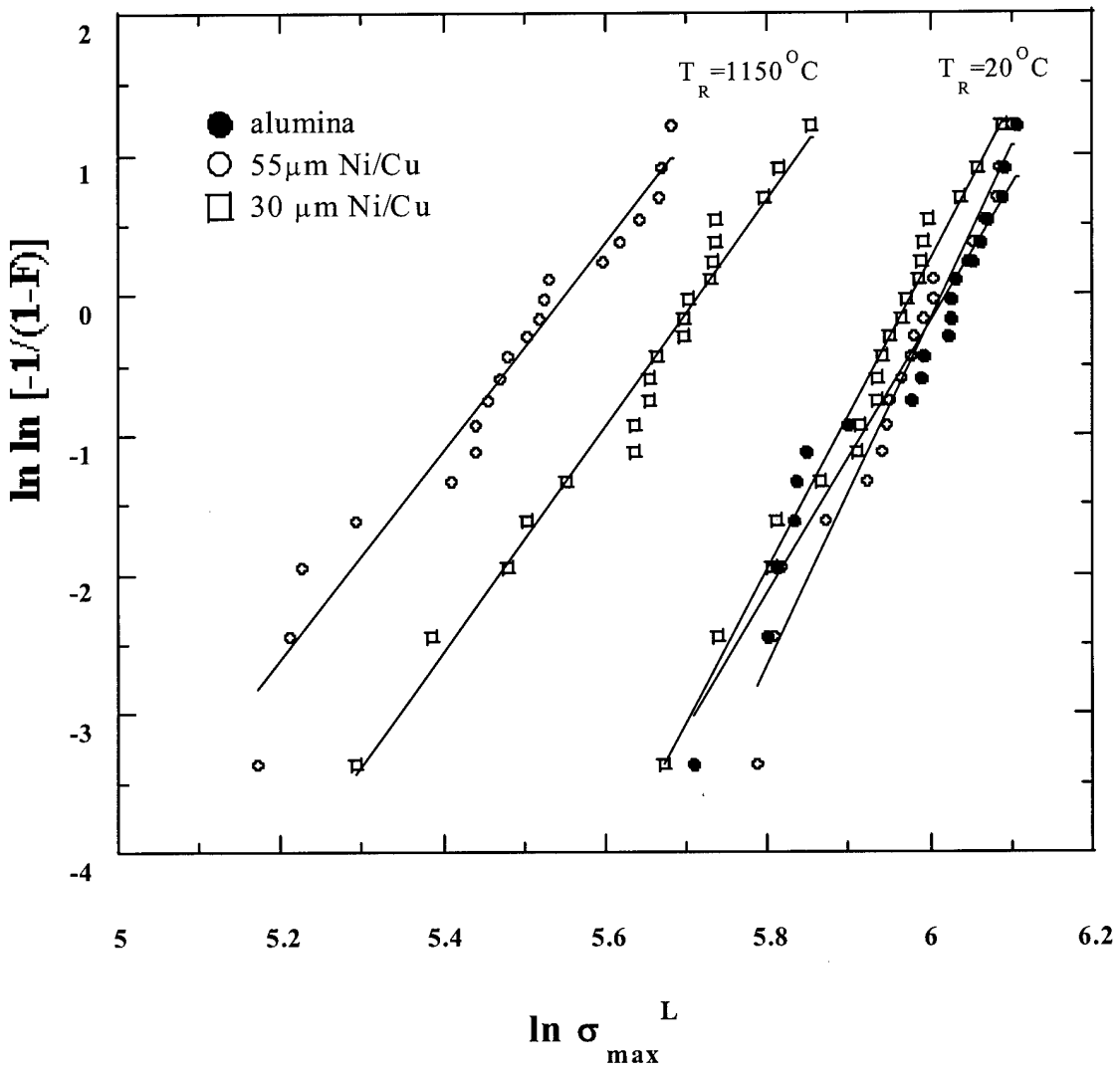
alumina
55μm Ni/Cu
30 μm Ni/Cu
T_R=1150°C
T_R=20°C
ln ln [-1/(1-F)]
ln σ_max^L
2
1
0
-1
-2
-3
-4
5
5.2
5.4
5.6
5.8
6
6.2

Fig. 3

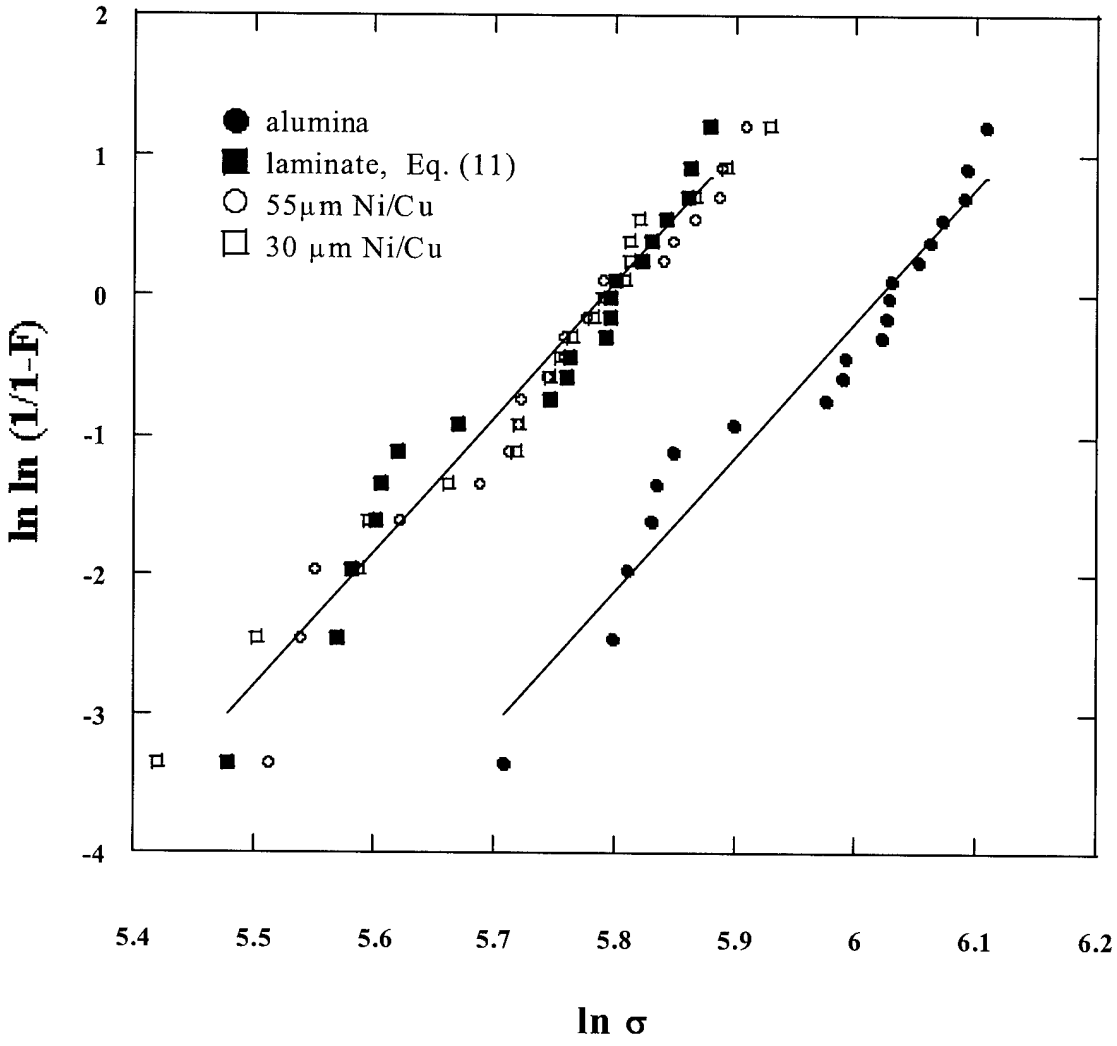
alumina
laminate, Eq. (11)
55μm Ni/Cu
30 μm Ni/Cu
ln ln (1/1-F)
ln σ
2
1
0
-1
-2
-3
-4
5.4
5.5
5.6
5.7
5.8
5.9
6
6.1
6.2

Fig. 4

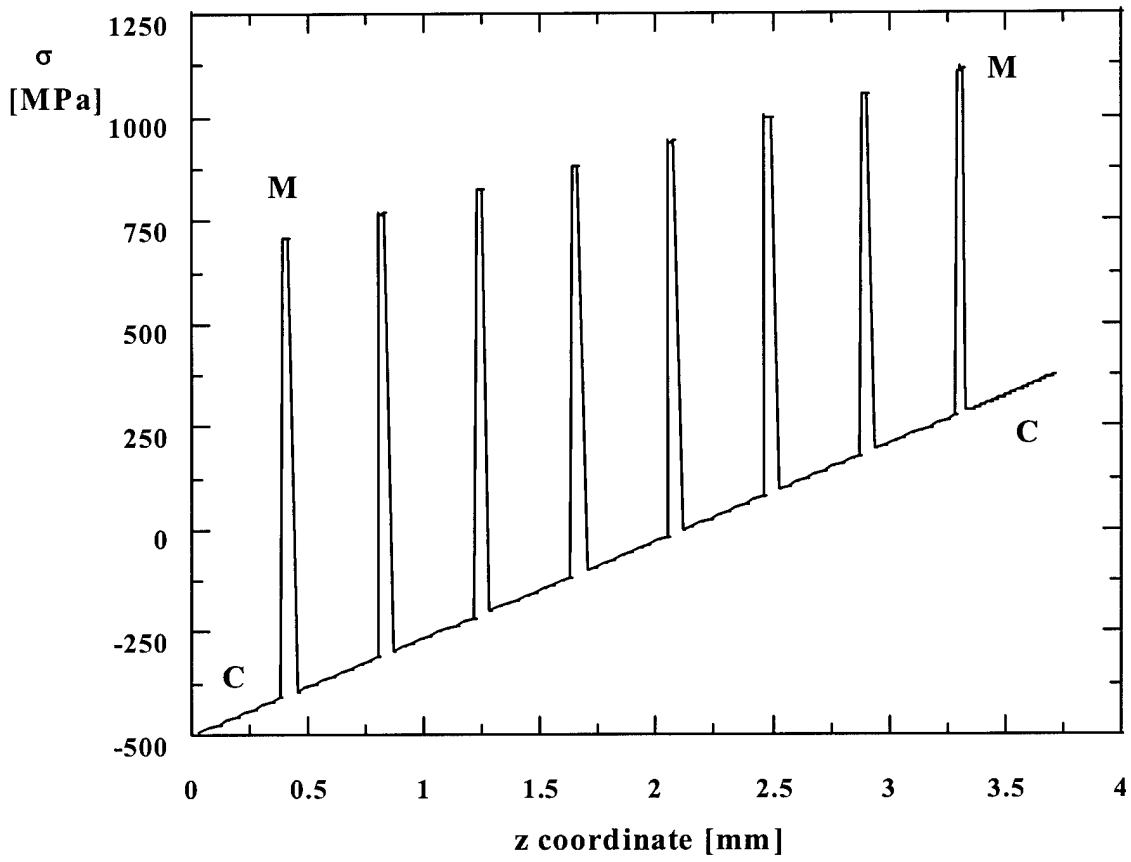
σ
[MPa]
1250
1000
750
500
250
0
-250
-500
M
M
C
C
0
0.5
1
1.5
2
2.5
3
3.5
4
z coordinate [mm]

Fig. 5